Research Paper

GEOSPHERE

GEOSPHERE; v. 12, no. 5

doi:10.1130/GES01315.1

15 figures; 1 table; 12 supplemental files

CORRESPONDENCE: ggehrels@gmail.com

CITATION: Pepper, M., Gehrels, G., Pullen, A., Ibanez-Mejia, M., Ward, K.M., and Kapp, P., 2016, Magmatic history and crustal genesis of western South America: Constraints from U-Pb ages and Hf isotopes of detrital zircons in modern rivers: Geosphere, v. 12, no. 5, p. 1532–1555, doi:10.1130/GES01315.1.

Received 20 January 2016
Revision received 2 May 2016
Accepted 20 June 2016
Published online 22 July 2016

Magmatic history and crustal genesis of western South America: Constraints from U-Pb ages and Hf isotopes of detrital zircons in modern rivers

Martin Pepper, George Gehrels, Alex Pullen, Mauricio Ibanez-Mejia, Kevin M. Ward, and Paul Kapp

Department of Geosciences, University of Arizona, Tucson, Arizona 85721, USA

ABSTRACT

Western South America provides an outstanding laboratory for studies of magmatism and crustal evolution because it contains Archean–Paleoproterozoic cratons that amalgamated during Neoproterozoic supercontinent assembly, as well as a long history of Andean magmatism that records crustal growth and reworking in an accretionary orogen. We have attempted to reconstruct the growth and evolution of western South America through U-Pb geochronologic and Hf isotopic analyses of detrital zircons from 59 samples of sand mainly from modern rivers. Results from 5524 new U-Pb ages and 1199 new Hf isotope determinations are reported. Our data are integrated with previously published geochronologic and Hf isotopic information, yielding a combined record that includes >42,000 ages and >1900 Hf isotope analyses. These large data sets yield five main conclusions: (1) South America has an age distribution that is similar to most other continents, presumably reflecting processes of crustal generation and/or preservation related to the supercontinent cycle, with age maxima at 2.2–1.8 Ga, 1.6–0.9 Ga, 700–400 Ma, and 360–200 Ma; (2) <200 Ma magmatism in western South America has age maxima at ca. 183, 166, 149, 125, 110, 88, 65, 35, 21, and 4 Ma (with significant north-south and east-west variations), yielding an average cyclicity of ~33 m.y.; (3) for the past 200 m.y., no correlation exists between magmatism and the velocity of convergence between central South America and Pacific oceanic plates, the age of the downgoing plate, or the absolute motion of South America; (4) Hf isotopes record reworking of older crustal materials during most time periods, with incorporation of juvenile crust at ca. 1.6–1.0 Ga, 500–300 Ma, and ca. 175–35 Ma; and (5) the Hf isotopic signature of <200 Ma magmatism is apparently controlled by the generation of evolved crust during crustal thickening and eastward arc migration, versus juvenile magmas during extensional tectonism and westward and/or outboard migration of arc magmatism.

INTRODUCTION

Understanding the generation and reworking of continental crust has been a long-standing goal in Earth science (Armstrong, 1968). Western South America provides an excellent laboratory for studying crustal evolution because it contains older cratons that record Precambrian crustal genesis and assembly and also early Paleozoic through modern magmatic assemblages that formed along the Andean convergent and/or accretionary plate boundary (Cordani et al., 2000; Aceñolaza et al., 2002; Cawood, 2005; Franz et al., 2006; Cawood and Buchan, 2007; Ramos, 2009). This history has been reconstructed through a large number of detailed studies of specific areas (e.g., Bahlburg and Hervé, 1997; Loewy et al., 2004; Hervé et al., 2007; Augustsson and Bahlburg, 2008; Chew et al., 2008; Bahlburg et al., 2009, 2011; Miskovic et al., 2009), as well as several syntheses that have focused on assembly of South America (e.g., Goodwin, 1996) and evolution of the Andean margin (e.g., Aceñolaza et al., 2002; Haschke et al., 2002; Cediel et al., 2003; Cawood, 2005; Kay et al., 2005; Franz et al., 2006; Cawood and Buchan, 2007).

This study attempts to reconstruct the magmatic history and crustal evolution of western South America through U-Pb geochronologic and Hf isotopic analysis of detrital-zircon grains from 59 samples of modern sediment (Fig. 1). These new data are combined with previously published age and Hf isotope information, resulting in a compilation with >42,000 ages and >1900 Hf isotope determinations. In an effort to analyze these large data sets quantitatively, we (1) use maximum likelihood estimation to determine the main age groups present in age distributions, (2) evaluate possible cyclicity of magmatic records using a Lomb-Scargle least-squares spectral analysis and a continuous wavelet transform (CWT) analysis, (3) investigate possible connections between plate motions and magmatic records using cross wavelet transform and wavelet coherence analyses, and (4) use least-squares regression analysis to determine Hf isotope evolution trajectories.

Quantitative analysis of these U-Pb and Hf isotopic data sets provides new insights into the magmatic history and crustal evolution of western South America. All of the records reveal cyclic patterns that relate to the supercontinent cycle for longer time scales and, for the past 200 m.y., record changes in the tectonic setting of Andean arc magmatism. Interestingly, our data do not record cycles of Andean crustal evolution on a 30–50 m.y. time scale, which have been fundamental to recent discussions of orogenic cyclicity (e.g., Haschke et al., 2002, 2006; DeCelles et al., 2009, 2015; Ramos, 2009).

Combined U-Pb geochronology and Hf isotope analysis of zircon is a powerful method for evaluating regional patterns of magmatic history and crustal evolution due to the power of sedimentary averaging (Link et al.,

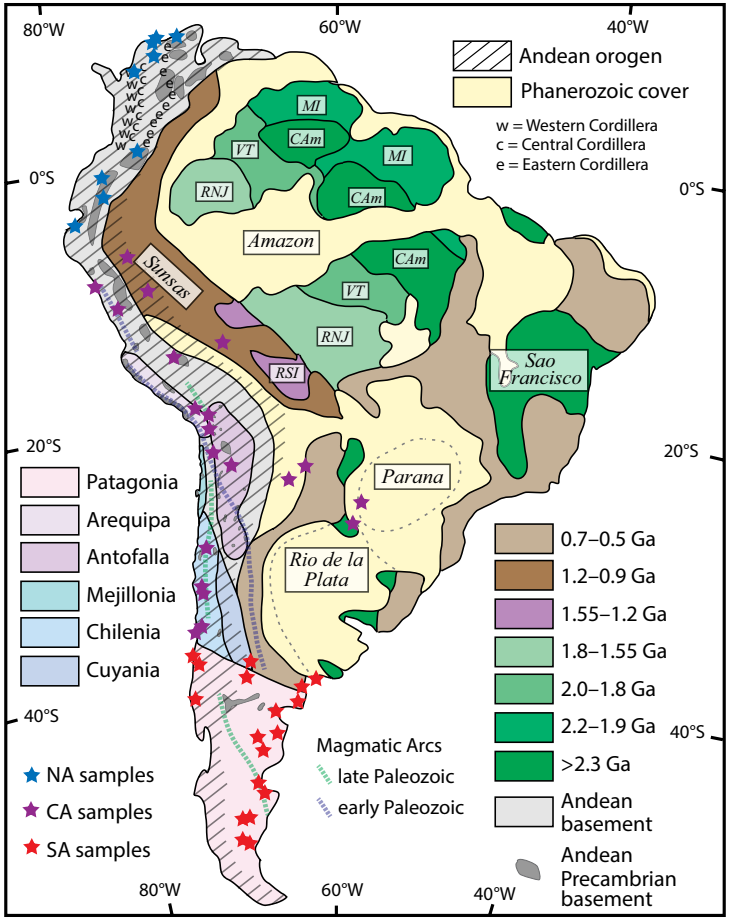

Figure 1. Map showing first-order geologic features of South America (adapted from Goodwin, 1996; Ramos, 2008, 2009, 2010; Bahlburg et al., 2009). Samples are keyed to three regions as follows: northern Andes (NA; 12°N–4°S), central Andes (CA; 4°S–34°S), and southern Andes (SA; 34°S–54°S). Abbreviations: CAm—Central Amazon craton; MI—Maroni-Itacaiunas province; RNJ—Rio Negro Juruena mobile belt; RSI—Rondonian San Ignacio province; VT—Ventuari-Tapajos province.

2005), the durability of zircon under most crustal pressure-temperature (P-T) conditions (Speer, 1982), the ability of U-Pb geochronology to record ages of felsic to intermediate-composition magmatism (e.g, Condie et al., 2011), and the petrogenetic information provided by Hf isotopes (e.g, Augustsson et al., 2006; Bahlburg et al., 2009, 2011; Hawkesworth et al., 2010; Collins et al., 2011; Dhuime et al., 2011). It is important to note, however, that the age and Hf isotopic signature of detrital zircons provides a somewhat biased record of magmatic history and crustal evolution. A more complete analysis would require consideration of (1) variations in zircon abundance related to rock composition (e.g., SiO_2 and/or Zr content) (Moecher and Samson, 2006; Dickinson, 2008), (2) three-dimensional analysis of the volumes of igneous rock present in the Andes through time (e.g., Paterson and Ducea, 2015), (3) igneous rocks that lack zircon, and (4) the importance of crustal additions and removals arising from tectonic processes (e.g., terrane accretion, subduction erosion, and delamination and/or relamination) and erosion. Such analyses are beyond the scope of this paper but will be facilitated by the new and compiled information presented herein.

Our study complements the work of Rino et al. (2004, 2008), Condie et al. (2005, 2009), Mapes et al. (2005), and Iizuka et al. (2010), who presented ages of detrital zircons from modern sand samples along the Amazon and Paraná Rivers. To complement the information from large rivers, we include samples from numerous smaller river systems (e.g., Milliman and Syvitski, 1992) that are present along the eastern and western flanks of the modern Andes.

GEOLOGICAL FRAMEWORK OF SOUTH AMERICA

The South American continent consists, to first order, of several Archean–Paleoproterozoic cratons that were effectively welded together during Mesoproterozoic through early Paleozoic orogenesis (Goodwin, 1996). This continental cratonic nucleus served as the backstop for accretionary processes that formed the Andean orogen along the paleo-Pacific margin (Coney, 1992; Cawood, 2005; Cawood and Buchan, 2007). The following sections outline the geologic evolution of cratonal South America and the northern, central, and southern Andes, with an emphasis on patterns of magmatism and crustal generation and/or reworking (Fig. 1).

Cratonal Nucleus

The nucleus of South America consists mainly of the Amazon, Sao Francisco, Parana, and Rio de la Plata cratons (Fig. 1). The Central Amazon craton (CAm) has Archean ages of 3.3–2.5 Ga. The Maroni-Itacaiunas province (MI) occurs east of the CAm with radiometric ages between 2.2 and 1.9 Ga. Westward, the Ventuari-Tapajos (VT) mobile belt (2.0–1.8 Ga) and the Rio Negro Juruena mobile belt (RNJ; 1.8–1.6 Ga) formed during the accretion of intraoceanic arcs. The Rondonian San Ignacio (RSI) province (1.6–1.3 Ga) consists of accreted arc terranes and microcontinents that experienced high-grade metamorphism during Mesoproterozoic time (Teixeira et al., 1989; Tassinari and Macambira, 1999; Santos et al., 2000, 2008; Cordani and Teixeira, 2007; Cordani et al., 2009). Along the western margin of the Amazon craton is the Sunsas orogen, which yields ages between 1.2 and 0.9 Ga (Litherland and Power, 1989; Teixeira et al., 2010; Ibanez-Mejia et al., 2011). Separating these cratons are the Brasiliano mobile belts, with dominant magmatism during

Neoproterozoic–earliest Paleozoic (0.7–0.5 Ga) time (Goodwin, 1996; Rapela et al., 1998, 2007; Kröner and Cordani, 2003; Valeriano et al., 2008; Cordani, 2009; Cordani et al., 2009).

Northern Andes

The northern Andes (NA) are divided into three separate mountain ranges that consist mainly of Precambrian basement (Cordani et al., 2005; Ordóñez-Carmona et al., 2006; Ibanez-Mejia et al., 2011). The western Cordillera ("w" on Fig. 1) comprises oceanic magmatic and deep-marine sedimentary rocks of mainly Cretaceous age (McCourt et al., 1984; Cortés et al., 2005; Kennan and Pindell, 2009; Borrero et al., 2012). The main volcanic arc along the central Cordillera ("c" on Fig. 1) is composed mainly of Jurassic–Cretaceous igneous rocks intruded into and resting on both oceanic and continental crystalline basement (Aspden and McCourt, 1986; Aspden et al., 1987; Cediel et al., 2003). The eastern Cordillera ("e" on Fig. 1) consists of Archean–Mesoproterozoic inliers surrounded by 1.1–1.0 Ga rocks (Restrepo-Pace et al., 1997; Ruiz et al., 1999; Cordani et al., 2005; Jiménez-Mejía et al., 2006; Ordóñez-Carmona et al., 2006; Chew et al., 2007a, 2007b, 2008; Cardona et al., 2009; Miskovic et al., 2009; Ibanez-Mejia et al., 2011).

Central Andes

The central Andes (CA) consist of arc-type and basinal assemblages that formed in a convergent-margin setting from early Paleozoic time to the recent. Some of these assemblages may be exotic to South America (e.g., Cuyania terrane; Astini and Thomas, 1999; Ramos, 2004; Thomas et al., 2004; Finney, 2007), whereas most formed during long-lived accretionary tectonism along the proto-Andean margin (Cawood, 2005). Some terranes contain crystalline basement of Paleo- or Meso-Proterozoic age (Shackleton et al., 1979; Loewy et al., 2004; Chew et al., 2007a) or of Neoproterozoic age (Jordan and Allmendinger, 1986; Strecker et al., 1989; Allmendinger et al., 1997; Escayola et al., 2007).

Southern Andes

The southern Andes (SA) consist primarily of Proterozoic and Paleozoic rocks exposed in basement uplifts (Pankhurst et al., 2000, 2006; Augustsson et al., 2006), rimmed to the west by post-Triassic magmatic rocks of the Andean orogen (Kay et al., 2005; Hervé et al., 2007). The southern portion of SA belongs to the Patagonia microcontinent, which consists of widespread Paleozoic magmatic arc and basinal assemblages that formed in the broad accretionary Terra Australis orogen (Coney, 1992; Stern and De Wit, 2003; Cawood and Buchan, 2007; Ramos, 2008; Barbeau et al., 2009).

PRESENT STUDY

Sampling Methodology

Samples were collected from active channels of modern rivers and from beaches along shorelines. Most of the rivers sampled do not have dams or major construction projects that could have influenced zircon age distributions. Each sample consisted of a mixture of sediment from multiples sites (within a ~10 m^2 area) with a wide range of grain sizes (silt to coarse sand). Material coarser than 2 mm was removed during sample collection. This strategy was followed in an effort to maximize the number of age groups recognized and reduce biases from hydrodynamic sorting (Garzanti et al., 2009; Lawrence et al., 2011). Heavy minerals from each composite sample were initially concentrated with a gold pan, and then zircons were extracted using a Frantz isodynamic separator and heavy liquids (techniques described by Gehrels, 2000).

Sample Descriptions

Fifty-nine samples were collected from rivers draining the northern, central, and southern Andes and from beach deposits near river deltas (Fig. 1 and Table 1).

Northern Andes

Thirteen samples were collected from the northern Andes (NA) as follows. Sample NA01 was collected from the Caribbean coast. Seven samples were collected from the Magdalena River system in the Magdalena Valley (separating the eastern and central Cordilleras of Fig. 1), with NA02 from lowlands 140 km upstream, NA03 and NA04 from the Magdalena delta, NA05 along the coast 70 km west of the Magdalena delta, and NA06–NA09 from the flanks of the eastern and western Cordillera (EC and WC) in the Magdalena highlands. Four samples were collected farther south, with NA10 from the Andean highlands, NA11 from a tributary of the Amazon River system, and NA12 and NA13 along the western flank of the western Cordillera ("w" on Fig. 1).

Central Andes

Twenty-five samples were collected from both the western and eastern flanks of the central Andes (CA), with a spacing of ~300–400 km. Along the eastern flank of the Andes, CA01–CA04 were collected from tributaries of the Rio de la Plata river system, CA05 and CA06 are from tributaries of the Amazon river system, CA07 and CA08 are from the Andean highlands, and CA09 and CA10 are from southern Amazon tributaries. Along the western flank of the Andes, samples CA11–CA22 were collected from small perennial rivers near the Atacama Desert. CA16 and CA23 are from beach sands to the west.

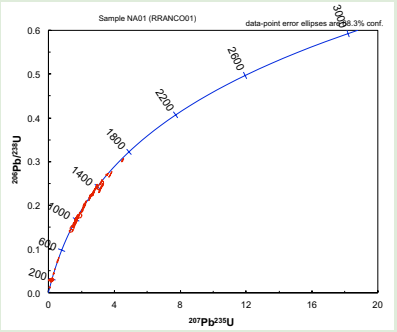

[1]Supplemental Data 1. U-Pb data tables of northern Andes region. Please visit http://dx.doi.org/10.1130/GES01315.S1 or the full-text article on www.gsapubs.org to view the Supplemental Data.

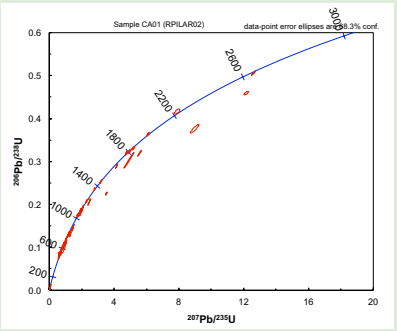

[2]Supplemental Data 2. U-Pb data tables of central Andes region. Please visit http://dx.doi.org/10.1130/GES01315.S2 or the full-text article on www.gsapubs.org to view the Supplemental Data.

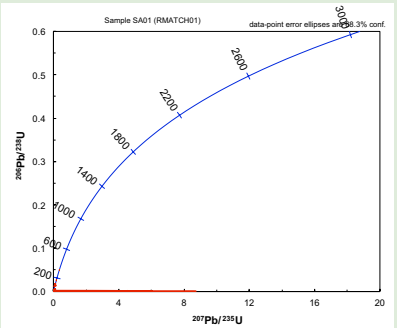

[3]Supplemental Data 3. U-Pb data tables of southern Andes region. Please visit http://dx.doi.org/10.1130/GES01315.S3 or the full-text article on www.gsapubs.org to view the Supplemental Data.

TABLE 1. SAMPLE INFORMATION

ID	Sample name	Sand type	No. of analyses U-Pb/Hf
Northern Andes (NA)			
NA01	RRANCO01	Delta	100/28
NA02	RMAGCO06	River	102/23
NA03	RMAGCO07	Delta	101/20
NA04	RMAGCO08	Delta	97/20
NA05	RSINCO01	River	106/23
NA06	RCHICO01	River	101/20
NA07	RNEICO01	River	106/24
NA08	RMAGCO01	River	92/20
NA09	RPAICO01	River	93/27
NA10	RCHOTEC01	River	99/20
NA11	RBLAEC01	River	80/15
NA12	RTENEC01	River	69/21
NA13	RJUBEC01	River	103/25
NA14	RSULPE01	River	88/23
Central Andes (CA)			
CA01	RPILAR02	River	74/17
CA02	RBERAR02	River	95/20
CA03	RPILAR01	River	76/20
CA04	RBERAR01	River	81/13
CA05	RHUALPE01	River	96/20
CA06	RPUCPE01	River	97/20
CA07	RHUANPE01	River	91/22
CA08	RLUNPE01	River	100/20
CA09	RMDDPE01	River	92/20
CA10	RAQUIPE01	River	100/23
CA11	RTRUPE01	River	100/21
CA12	RHUAPE01	River	107/21
CA13	RCLAPE01	Beach	101/21
CA14	RICAPE01	River	78/20
CA15	ROCOPE01	River	97/22
CA16	BILOPE01	River	99/22
CA17	RLLUCH01	River	96/20
CA18	RCAMCH01	River	106/25
CA19	RLOACL01	River	79/17
CA20	RLOACL02	Beach	85/18
CA21	RCONCH01	River	104/18
CA22	RCHOCH01	River	106/9
CA23	BVILCH01	River	112/19

(*continued*)

TABLE 1. SAMPLE INFORMATION (*continued*)

ID	Sample name	Sand type	No. of analyses U-Pb/Hf
Southern Andes (SA)			
SA01	RMATCH01	River	93/20
SA02	RMAUCH01	River	94/25
SA03	RBIOCH01	Delta	87/27
SA04	RBIOCH02	River	99/17
SA05	RBUECH01	River	94/18
SA06	RCOLAR01	River	86/20
SA07	RCOLAR02	River	94/27
SA08	RSAUAR01	River	93/21
SA09	RNEUQAR01	River	101/20
SA10	RLIMAR01	River	93/18
SA11	RNEGAR01	River	100/19
SA12	RNEGAR02	River	104/21
SA13	ASALAR01	River	100/25
SA14	RCHUAR01	River	99/16
SA15	RCHUAR02	River	107/25
SA16	RCHIAR01	River	104/23
SA17	RDESAR01	Arroyo	99/26
SA18	RDESAR02	Arroyo	95/17
SA19	RCHIAR02	River	93/22
SA20	RSCRAR01	River	59/16
SA21	RGALAR01	River	97/20
SA22	RCHIAR03	River	22/1

Southern Andes

Five southern Andes (SA) samples (SA01–SA05) were collected from the western flank of the orogen from rivers with a spacing of ~300 km. Samples SA01 and SA02 are from perennial rivers within 10 km of the coast, whereas sample SA03 was collected from the coast and SA04 was collected farther upstream. Samples SA06–SA22 are from the eastern flank of the Andes, with a spacing of ~200 km. These samples are from lowland portions of rivers, ~30–50 km from the Atlantic coast.

U-Pb Analytical Methods

Uranium-lead geochronology of zircons was conducted by laser ablation–multicollector–inductively coupled plasma mass spectrometry (LA-MC-ICPMS) at the Arizona LaserChron Center (www.laserchron.org) using analytical methods described by Gehrels (2000), Gehrels et al. (2006, 2008), and Gehrels and Pecha (2014). Cathodoluminescence (CL) images, acquired with a Gatan Chroma CL2 system (www.geoarizonasem.org), were used to ensure that analyses were conducted on homogeneous (generally interior) portions of zircon grains.

The U-Pb analytical data are reported in Supplemental Data 1–3[1,2,3]. These tables present the isotopic ratios, concentrations, calculated ages, and uncertainties for each analysis. Uncertainties are reported at 1-sigma, and include only internal uncertainty components (measurement of $^{206}Pb^*/^{238}U$, $^{206}Pb^*/^{207}Pb^*$, $^{206}Pb^*/^{204}Pb$) and a factor to incorporate the overdispersion of primary standard analyses. External (systematic) uncertainties are reported for each sample (at 2-sigma) in Supplemental Data 1–3 (see footnotes 1–3) and include contributions from the scatter of primary standard analyses, composition of common Pb, age of the primary standard, and U decay constants. Also reported for each analysis is the "best age," which is based on $^{206}Pb^*/^{238}U$ for <900 Ma grains and $^{206}Pb^*/^{207}Pb^*$ for >900 Ma grains.

Following standard practice (e.g., Gehrels, 2012, 2014), the U-Pb data tables do not include analyses that are highly (>20%) discordant or highly (>10%) reverse discordant and analyses with >10% uncertainty. These filters are not applied to <600 Ma $^{206}Pb^*/^{207}Pb^*$ ages and <100 Ma $^{206}Pb^*/^{238}U$ ages. Also

included in Supplemental Data 1–3 (see footnotes 1–3) are Pb*/U concordia diagrams (from Ludwig, 2008) and age-distribution diagrams that sum all ages (and associated uncertainties) from a sample (or set of samples) into a single curve (from www.laserchron.org).

For interpretive purposes, U/Th ratios for each analysis are reported in Supplemental Data 1–3 (see footnotes 1–3). Most (>90%) analyses have U/Th in the range of typical igneous values (e.g., 1–10; Rubatto, 2002), which are interpreted to record episodes of igneous activity. Values >10 are interpreted as possibly of metamorphic origin (e.g., Gehrels et al., 2009).

Hf Analytical Methods

Hafnium analyses were also conducted by LA-MC-ICPMS at the Arizona LaserChron Center, using methods described by Cecil et al. (2011) and Gehrels and Pecha (2014). Laser ablation analyses were conducted with a laser beam diameter of 40 microns, with ablation pits located either on top of the U-Pb analysis pits or adjacent to the U-Pb pits but in the same domain (using CL images as guides). Each acquisition consisted of one 40-second integration on backgrounds (on peaks with no laser firing) followed by 60 one-second integrations with the laser firing. The isotope ratios and uncertainties reported are based on all measurements, with only a 2-sigma filter to remove outliers. Critical isotope ratios used in data reduction are as follows: $^{179}Hf/^{177}Hf$ = 0.73250 (Patchett and Tatsumoto, 1980); $^{173}Yb/^{171}Yb$ = 1.132338 (Vervoort et al., 2004); $^{176}Yb/^{171}Yb$ = 0.901691 (Vervoort et al., 2004; Amelin and Davis, 2005); $^{176}Lu/^{175}Lu$ = 0.02653 (Patchett, 1983); and the decay constant of ^{176}Lu = 1.867e-11 (Scherer et al., 2001; Söderlund et al., 2004). Hafnium-depleted mantle model ages are not calculated because of uncertainties in the $^{176}Hf/^{177}Hf$ and $^{176}Lu/^{177}Hf$ of source material(s) from which the zircons crystallized.

Analyses were calibrated using solution analyses of JMC475, solutions of JMC475 mixed with varying concentrations of ^{176}Lu and ^{176}Yb, and laser ablation analyses of standard zircons Mud Tank, 91500, Temora2, R33, FC1, and Plesovice. Solutions of JMC475 yielded a weighted mean value of 0.282156 ± 0.000007 (2σ, n = 17). Solutions mixed with ^{176}Yb and ^{176}Lu [with $^{176}(Yb + Lu)/^{176}Hf$ up to 1.6] yielded a similar weighted mean value of 0.282150 ± 0.000008 (2σ, n = 16) with $^{173}Yb/^{171}Yb$ adjusted to 1.132423 (from value of 1.132338 suggested by Vervoort et al., 2004) to alleviate a slight correlation between measured $^{176}Hf/^{177}Hf$ and $^{176}(Yb + Lu)/^{176}Hf$.

Zircon standards yielded measured $^{176}Hf/^{177}Hf$ values that were slightly lower than the reported values. With measured values increased by 0.8 epsilon units, the following results were obtained:

- Mud Tank: weighted mean value of 0.282518 ± 0.000007 (2σ, n = 138) compared with reported value of 0.282507 (Woodhead and Hergt, 2005). This yields an offset of +0.4 epsilon units.
- 91500: weighted mean value of 0.282292 ± 0.000021 (2σ, n = 33) compared with reported value of 0.282313 (Fisher et al., 2014). This yields an offset of –0.7 epsilon units.
- Temora2: weighted mean value of 0.282677 ± 0.000009 (2σ, n = 33) compared with reported value of 0.282686 (Fisher et al., 2014). This yields an offset of –0.3 epsilon units.
- Plesovice: weighted mean value of 0.282480 ± 0.000007 (2σ, n = 125) compared with reported value of 0.282484 (Slama et al., 2008). This yields an offset of –0.1 epsilon units.
- FC1: weighted mean value of 0.282170 ± 0.000009 (2σ, n = 132) compared with reported value of 0.282183 (Fisher et al., 2014). This yields an offset of –0.4 epsilon units.
- R33: weighted mean value of 0.282735 ± 0.000009 (2σ, n = 148) compared with reported value of 0.282764 (Fisher et al., 2014). This yields an offset of –1.0 epsilon units.

These offsets suggest that the accuracy (external reproducibility) of a set of analyses is 1–2 epsilon units. The precision (internal reproducibility) of individual analyses is ~3 epsilon units, as indicated by an average measurement uncertainty of 2.8 epsilon units (average standard deviation of all standard measurements, at 2σ), and an average standard deviation for measurements of each standard of 2.8 epsilon units (at 2σ).

Data from all unknowns have been adjusted using a correction factor of +0.8 epsilon units and the revised $^{173}Yb/^{171}Yb$ value reported above.

Statistical Analyses

Three different statistical methods have been applied to analyze patterns and potential correlations among the geochronologic, isotopic, and plate motion data presented herein.

In an effort to characterize patterns of magmatism, we use a maximum likelihood analysis (from Unmix routine of Isoplot; Ludwig, 2008) to characterize the age and variation of overlapping ages. This method fits a Gaussian distribution to a set of ages and returns the mean and standard deviation of the constituent ages. The standard deviation is expressed at the 2σ level to characterize the range of included ages.

To investigate the cyclicity of magmatic records and plate convergence rates, we apply a Lomb-Scargle least-squares spectral analysis (Lomb, 1976; Scargle, 1982) to the geographically organized age distributions and the relative plate convergence rates of Maloney et al. (2013). Although the Lomb-Scargle least-squares spectral analysis is typically used to estimate periodicity of irregularly sampled data, the Lomb-Scargle method has some advantages (e.g., data vector can be irregularly sampled, data vector can have any length, and periodograms have known statistical properties) over the more common Fourier power spectral density (PSD) analysis. We note that although we prefer the Lomb-Scargle analysis, our data sets have a regular sampling interval (1 m.y.), and a Fourier PSD analysis produces a similar estimate of the PSD. Since we are comparing time series that measure different physical properties, we are not interested in the absolute power of each time series but in the relative peaks in periodicity between time series. To highlight any potential cyclical

correlations between these time series, we normalize each PSD estimate setting the maximum power observed for each time series equal to one.

We also explore potential correlations between plate convergence rates and the Andean magmatic history by first employing a sophisticated continuous wavelet transform (CWT) analysis to each of the individual records. Traditional Fourier analysis implicitly assumes any physical relationships are stationary in time. The wavelet method has several advantages over traditional Fourier analysis and is particularly well suited for analyzing geological and geophysical time series that may exhibit periodic behavior that varies in time with localized intermittent periodicities (Torrence and Compo, 1998). For each individual time series, we calculate the continuous (local) wavelet power spectrum. Because the wavelet is not everywhere localized in time, we define a cone of influence (COI), outside of which edge effects are significant. We also define a ≥95% confidence interval using a first-order autoregressive process (Allen and Smith, 1996) that models red noise (random walk noise) to identify statistically significant areas of signal-generated wavelet power. The continuous (local) wavelet power spectrum results for each individual time series show signal power at similar periods as the Lomb-Scargle periodograms and also contain additional information about localized intermittent periodicities.

The CWT analyses described above provide statistically significant information about localized intermittent periodicities. To explore potential mechanistic explanations of the magmatic records from South America, we employ two approaches of analyzing pairs of CWTs generated from individual time series—the cross wavelet transform (XWT) and the wavelet coherence (WTC). Here we briefly describe these two approaches and refer the interested reader to Grinsted et al. (2004) for a more detailed formal mathematical description. The XWT provides a statistically significant measure (≥95% confidence interval against red noise) of the common power between two CWTs as a function of period and time. Both the XWT and WTC have the additional property of returning the phase difference between signals with common power and/or coherence, also as a function of period and time. This information is helpful in establishing a mechanistic connection as any cause and effect relationship would be phase locked, meaning the phase (time lag) would be constant for any period with statistically significant common power and/or coherence. The WTC extends the analysis of XWT to time series with significant coherence even if the common power is low. The WTC is analogous to traditional correlation coefficients with the added property of quantifying correlation within localized intermittent periodicities.

RESULTS

U-Pb Geochronology

A total of 5524 new U-Pb analyses are reported in Supplemental Data 1–3 (see footnotes 1–3). Figure 1 shows the location of each sample on a geologic map of South America, and Supplemental Item 1[4] provides a description of the zircon grains present in each sample. Highlights of the results from samples from northern, central, and southern regions are described in following sections and shown on Figures 2–4. Figures 5 and 6 summarize the U-Pb age distributions from each region, with all age distributions smoothed using a sliding window that averages each set of five closest ages.

Northern Andes

Samples from the northern Andes (NA) contain detrital zircons that are quite variable in age (Fig. 2). Most samples contain a few ages between ca. 2.1 and ca. 1.7 Ga. The only age group present in most samples ranges from ca. 1.6 Ga to ca. 950 Ma, with dominant ages near ca. 1.0 Ga. Several samples contain grains of 700–400 Ma, and most samples contain abundant <400 Ma grains. The dominant ages for <200 Ma grains are shown on Figures 5 and 6.

Central Andes

For >200 Ma ages, the age patterns in the central Andes (CA; Fig. 3) generally resemble age patterns from regions to the north (Fig. 2), although proportions of the main age groups are somewhat different (Figs. 5 and 6). Namely, most samples are missing the ca. 1.6 Ga to ca. 950 Ma and 400–200 Ma age groups. Similarly, for <200 Ma ages, some age groups (e.g., those with peak ages of ca. 183 and ca. 126 Ma) are also missing from CA, and the proportions of other age groups are somewhat different (Figs. 5 and 6). The 600–400 Ma age group is much more prominent in the CA than the NA.

Southern Andes

The southern Andes (SA) yield age distributions that are quite different from NA and CA, with predominance of 400–250 Ma and <25 Ma grains in most samples and abundant 200–25 Ma ages in only three samples (Figs. 4–6). Southern Andes samples contain very few ages between 900 and 700 Ma and >1.2 Ga.

East-West Comparison of U-Pb Ages

As a complement to the above north-south comparison of ages, Figures 5 and 6 compare age distributions from rivers that are located along the eastern versus western flanks of the modern Andes. Omitted from this compilation are samples from rivers in the northernmost Andes (which drain northward) and in southern Patagonia (which have no sampled westerly counterparts). This comparison highlights the dominance of older basement sources in rivers of the eastern Andes versus the prevalence of Phanerozoic igneous rocks in the western Andes. This compilation also records a strong cyclicity to all records of Andean magmatism, which is explored in detail below.

Supplemental Item 1 (Zircon Properties)

SUPPLEMENTAL ITEM 1. PROPERTIES OF ZIRCON GRAINS IN EACH SAMPLE

Name	Sample	Lengthcm[2]	Grain Morphology[3]	Sorting[4]	Color[5]
NA01	RZANCO01	305	euhedral with some acicular	slightly mixed	light pink to golden
NA02	RMAGCO06	294	slightly rounded	very well mixed	clear to light pink
NA03	RMAGCO07	331	rounded	sorted	clear to light pink
NA04	RMAGCO08	258	rounded	well mixed	clear to light pink
NA05	RSINC001	330	mostly euhedral	mixed	mostly clear
NA06	RCHEC001	195	subrounded	well mixed	light pink and clear
NA07	RNEEC001	289	subrounded	slightly mixed	light pink
NA08	RMAGC001	218	slightly rounded	mixed	light pink to medium pink
NA09	RPAEC001	372	mostly euhedral	mixed	clear to medium brown
NA10	RCHOEC01	317	subrounded	well mixed	mostly clear
NA11	RTENEC01	306	mostly euhedral	well mixed	clear to light pink
NA12	RBLAEC01	287	slightly rounded	well mixed	some pink most clear
NA13	RJUBEC01	272	slightly rounded	mixed	light pink
NA14	RSULPI01	348	mostly euhedral	well mixed	light pink
CA01	RPILAR02	211	subrounded	mixed	mostly clear
CA02	RBERAR02	140	subrounded to rounded	fine grained unmixed sorted fine	clear to light pink
CA03	RPILAR01	174	subrounded to rounded	grained fine grained	clear
CA04	RBERAR01	141	subrounded	unmixed	clear to medium pink
CA05	RHUALPI01	250	rounded	slightly mixed	light pink
CA06	RPUCPI01	172	rounded	well mixed	clear to light pink
CA07	RHUANPI01	246	rounded	slightly mixed	light pink to pink
CA08	RLUNPI01	257	rounded	slightly sorted fine grained	mostly clear

[4]Supplemental Item 1. Zircon properties. Please visit http://dx.doi.org/10.1130/GES01315.S4 or the full-text article on www.gsapubs.org to view the Supplemental Item.

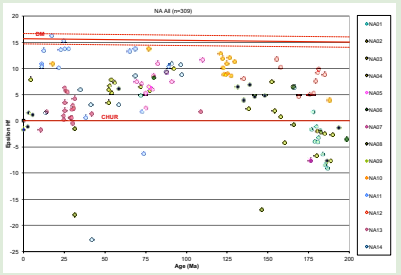

[5]Supplemental Data 4. Hf data tables of northern Andes region. Please visit http://dx.doi.org/10.1130/GES01315.S5 or the full-text article on www.gsapubs.org to view the Supplemental Data.

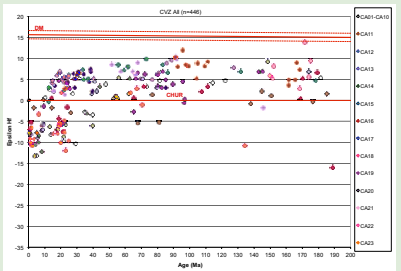

[6]Supplemental Data 5. Hf data tables of central Andes region. Please visit http://dx.doi.org/10.1130/GES01315.S6 or the full-text article on www.gsapubs.org to view the Supplemental Data.

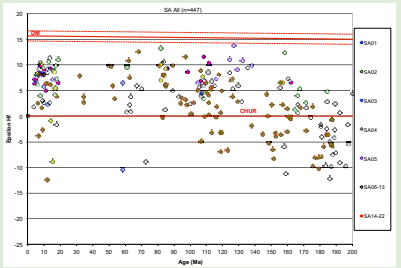

[7]Supplemental Data 6. Hf data tables of southern Andes region. Please visit http://dx.doi.org/10.1130/GES01315.S7 or the full-text article on www.gsapubs.org to view the Supplemental Data.

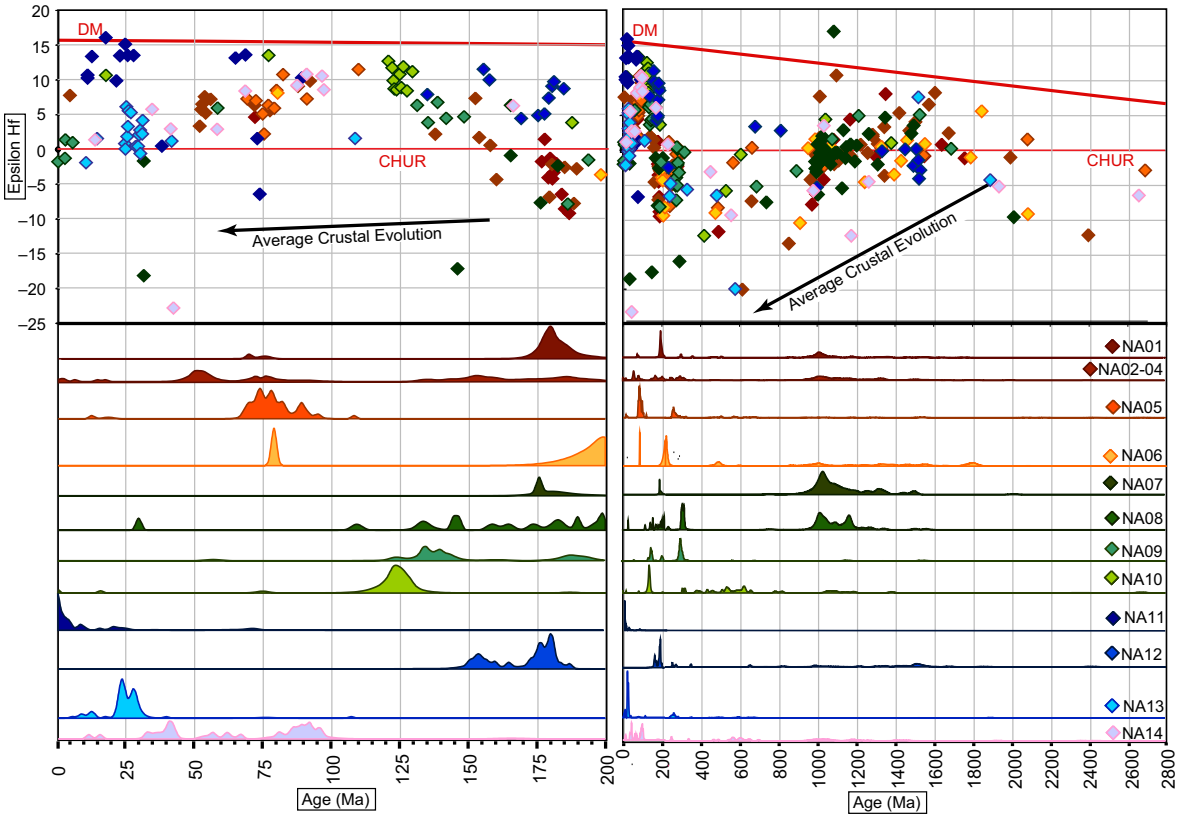

Figure 2. Diagram showing U-Pb and Hf isotopic results from northern Andes (NA) samples; 1339 U-Pb ages and 308 Hf isotope analyses are reported. Reference lines for Hf isotope data are as follows: DM—depleted mantle array, calculated using $^{176}Hf/^{177}Hf_0 = 0.283225$ and $^{176}Lu/^{177}Hf_0 = 0.03830$ (Vervoort and Blichert-Toft, 1999); CHUR—chondritic uniform reservoir, calculated using $^{176}Hf/^{177}Hf = 0.282785$ and $^{176}Lu/^{177}Hf = 0.0336$ (Bouvier et al., 2008). Arrows showing average crustal evolution represent trajectories with present-day $^{176}Lu/^{177}Hf = 0.0115$ (Vervoort and Patchett, 1996; Vervoort et al., 1999). The average measurement uncertainty for all NA analyses is 2.8 epsilon units (2σ). Age-distribution curves for 0–200 Ma and 200–2800 Ma have been normalized such that area under each curve is the same.

Hf Isotope Geochemistry

The results of our Hf isotope analyses are described in the following sections for samples from the northern, central, and southern Andes. A total of 1199 new analyses are reported in Supplemental Data 4–6[5,6,7]. These tables report all details of individual analyses and present plots with results from each sample. Results are summarized on Figures 2–4.

Northern Andes

Hafnium isotope data from the northern Andes are quite variable and record interesting patterns through time. As shown on Figure 2, εHf_t values progressively decrease (become more evolved) from ca. 1.6 Ga through ca. 400 Ma, increase (become more juvenile) from ca. 300 to ca. 100 Ma, and then in most cases become more evolved again after ca. 100 Ma (Fig. 2).

Central Andes

Analyses from the central Andes reveal a generally similar pattern of changing εHf_t values (Fig. 3). Additional patterns include the presence of more abundant >1.6 Ga grains with variable εHf_t values, more juvenile values for 1.2–1.0 Ga grains, a distinctive pull-down of 650–500 Ma values, and considerably more negative εHf_t values for the youngest grains.

Southern Andes

The southern Andes (Fig. 4) yield few >1.2 Ga grains, mostly juvenile 1.2–1.0 Ga grains, abundant 600–300 Ma grains with intermediate εHf_t values, values that increase from moderately negative to positive from 300 to 100 Ma, and then mostly positive values for <100 Ma grains.

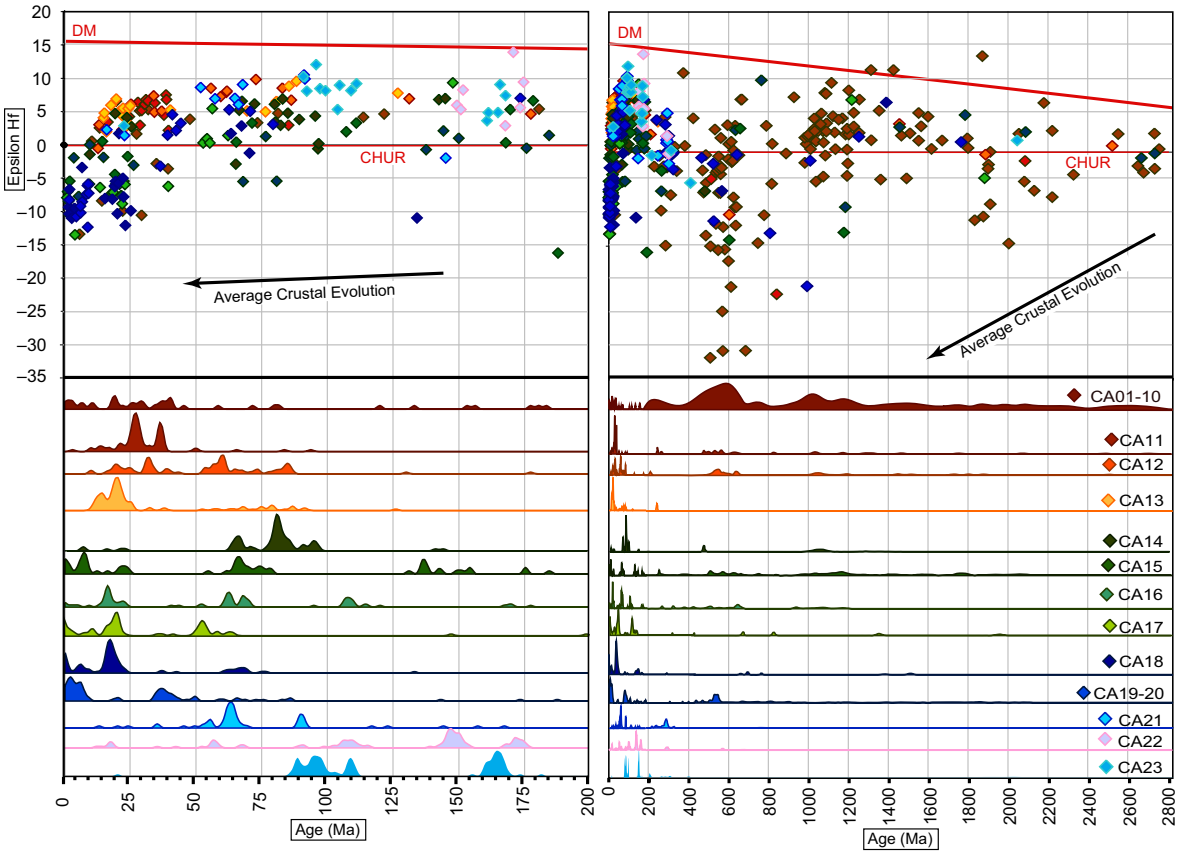

Figure 3. Diagram showing U-Pb and Hf isotopic results from central Andes (CA) samples; 2172 U-Pb ages and 447 Hf isotope analyses are reported. See Figure 2 for explanation. The average measurement uncertainty for all analyses is 2.6 epsilon units (2σ).

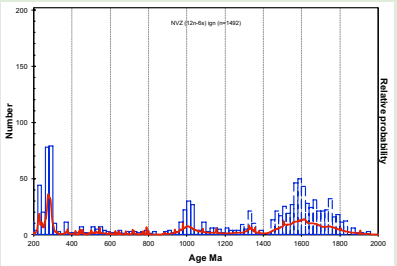

[8]Supplemental Data 7. Compilation of published U-Pb data. Please visit http://dx.doi.org/10.1130/GES01315.S8 or the full-text article on www.gsapubs.org to view the Supplemental Data.

1 **Supplemental Item 2 (List of references used for the South American radiometric ages**
2 **compilation)**
3 **Northern Andes DZ ages**
4 Ayala, R.C., Bayona, G., Cardona, A., Ojeda, C., Montenegro, O.C., Montes, C., Valencia, V.,
5 and Jaramillo, C., 2012, The paleogene synorogenic succession in the northwestern
6 Maracaibo block: Tracking intraplate uplifts and changes in sediment delivery systems:
7 Journal of South American Earth Sciences, v. 39, p. 93-111.
8 Bande, A., Horton, B.K., Ramírez, J.C., Mora, A., Parra, M., and Stockli, D.F., 2012, Clastic
9 deposition, provenance, and sequence of Andean thrusting in the frontal Eastern
10 Cordillera Llanos foreland basin of Colombia: Geological Society of America Bulletin,
11 v. 124, p. 59-76.

[9]Supplemental Item 2. U-Pb compilation references. Please visit http://dx.doi.org/10.1130/GES01315.S9 or the full-text article on www.gsapubs.org to view the Supplemental Item.

COMPARISON WITH EXISTING U-Pb AND Hf DATA FROM SOUTH AMERICA

U-Pb

In an attempt to compare our U-Pb geochronologic data set with previously published information, we have compiled ages reported from igneous and detrital samples from all of western South America (Figs. 5 and 6). All available U-Pb ages are included in the compilation, whereas only young (<200 Ma) volcanic K-Ar and Ar-Ar ages are included because of the likelihood that pre–200 Ma ages record cooling rather than igneous activity. Ages of individual analyses are included where reported; mean ages are reported where results from individual analyses are not available. Supplemental Data 7[8] includes all compiled ages and also a map that shows the distribution of sampled areas. The sources for the compiled data are listed in Supplemental Item 2[9]. A total of 26,851 detrital ages and 9929 igneous ages are included in this compilation, in addition to our 5524 new ages.

Comparisons between our detrital data, previously published detrital data from both sedimentary rocks and modern sediment, and igneous rocks are provided on Figure 6. This comparison shows that our data and previously reported detrital data are quite similar in the dominant ages recognized and in the approximate proportions of different age groups. These two data sets are somewhat different from the age distribution defined by igneous samples, presumably because of temporal and/or spatial biases in the selection of studied igneous suites.

Included in this compilation are analyses of detrital-zircon ages from several South American rivers. Condie et al. (2005, 2009) report ages from rivers in Brazil and Peru, whereas Iizuka et al. (2010) and Rino et al. (2004, 2008) report

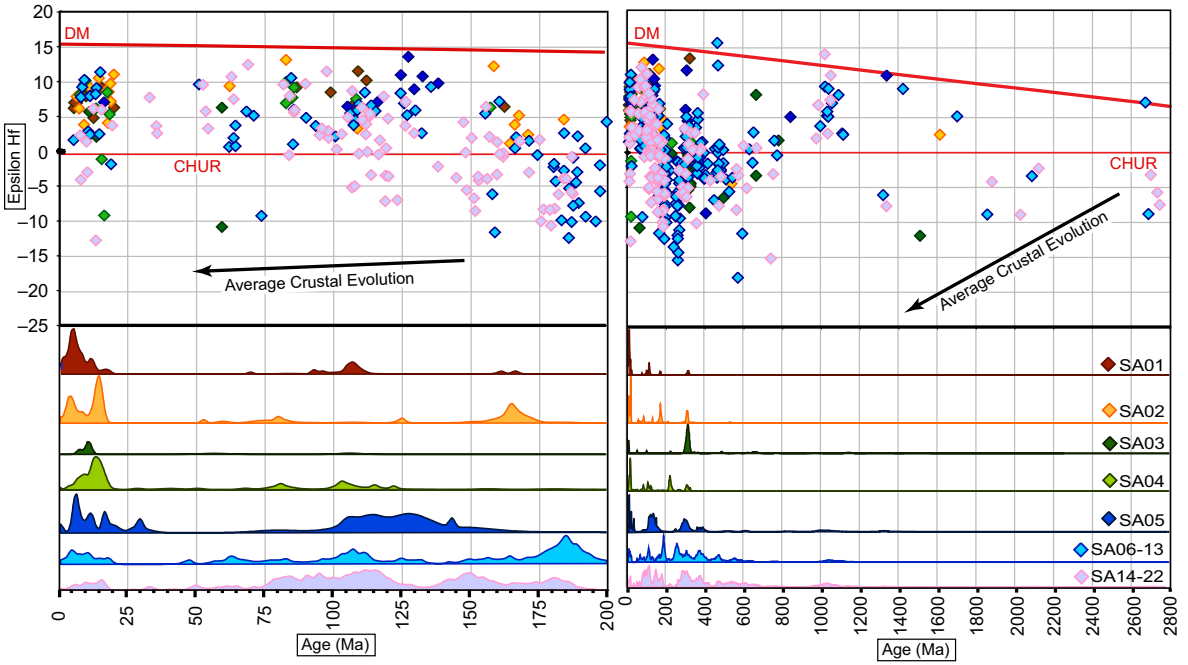

Figure 4. Diagram showing U-Pb and Hf isotopic results from southern Andes (SA) samples. 2013 U-Pb ages and 444 Hf isotope analyses are reported. See Figure 2 for explanation. The average measurement uncertainty for all analyses is 3.0 epsilon units (2σ).

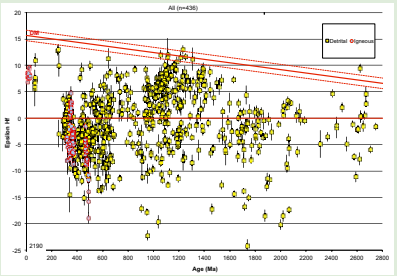

[10]Supplemental Data 8. Compilation of published Hf data. Please visit http://dx.doi.org/10.1130/GES01315.S10 or the full-text article on www.gsapubs.org to view the Supplemental Data.

1 **Supplemental Item 3 (References for information used in Hf isotope compilation)**

2 Augustsson, C., Muenker, C., Bahlburg, H., and Fanning, C.M., 2006, Provenance of late
3 Palaeozoic metasediments of the SW South American Gondwana margin: a combined U–
4 Pb and Hf-isotope study of single detrital zircons: Journal of the Geological Society, v.
5 163, p. 983-995.

6 Bahlburg, H., Vervoort, J.D., Du Frane, S.A., Bock, B., Augustsson, C., and Reimann, C., 2009,
7 Timing of crust formation and recycling in accretionary orogens: Insights learned from
8 the western margin of South America: Earth-Science Reviews, v. 97, p. 215-241.

[11]Supplemental Item 3. Hf compilation references. Please visit http://dx.doi.org/10.1130/GES01315.S11 or the full-text article on www.gsapubs.org to view the Supplemental Item.

ages from the Amazon and Parana rivers. Mapes et al. (2009) have also conducted analyses from Amazon River sediment, with analyses that are forthcoming. Campbell and Allen (2008) have included analyses from South American rivers in their database, but these ages have not been included in our compilation because sample locations were not reported.

Hf

Hafnium data were also compiled from previous studies that reported essential information about the analyses (e.g., instrumentation, methodology, and data reduction). The acceptable data are tabulated in Supplemental Data 8[10], with associated references reported in Supplemental Item 3[11]. No acceptable analyses are available for the northern Andes; 688 were found from the central Andes and 85 from the southern Andes.

INTERPRETATION OF RESULTS

Our new and compiled data provide significant new insights into the magmatic history and crustal evolution of western South America. Each of these aspects is described below.

Magmatic History

The U-Pb data presented herein, combined with existing geochronologic information (Supplemental Data 7 [see footnote 8]; Supplemental Item 2 [see footnote 9]) and interpretations (e.g., Bahlburg and Hervé, 1997; Baldwin et al., 1997; Haschke et al., 2002, 2006; Cediel et al., 2003; Franz et al., 2006; Pankhurst et al., 2006; DeCelles et al., 2009, 2015; Miskovic et al., 2009; Ramos, 2009; Ducea et al., 2015; Paterson and Ducea, 2015) provide important new information about the history of magmatism in western South America. This record is most relevant for igneous activity of felsic to intermediate composition, given that most of the information is derived from ages of zircon, and zircon is generally of low abundance in mafic magmas. As noted above, the connection between age distribution and magmatic addition is also complicated by potential variations in Zr content (and hence zircon fertility) through space and time, the long and complex history of uplift and erosion in the Andes, and potential additions to and removals from the system by tectonic and erosional processes.

Given the objective of reconstructing the magmatic history of western South America, with emphasis on both ages and proportions of magmatism, it is important to recognize that all three sets of information (our data, published detrital data, and published igneous data) have biases. For igneous ages, it is clear that the age distribution is controlled in large part by the geographic

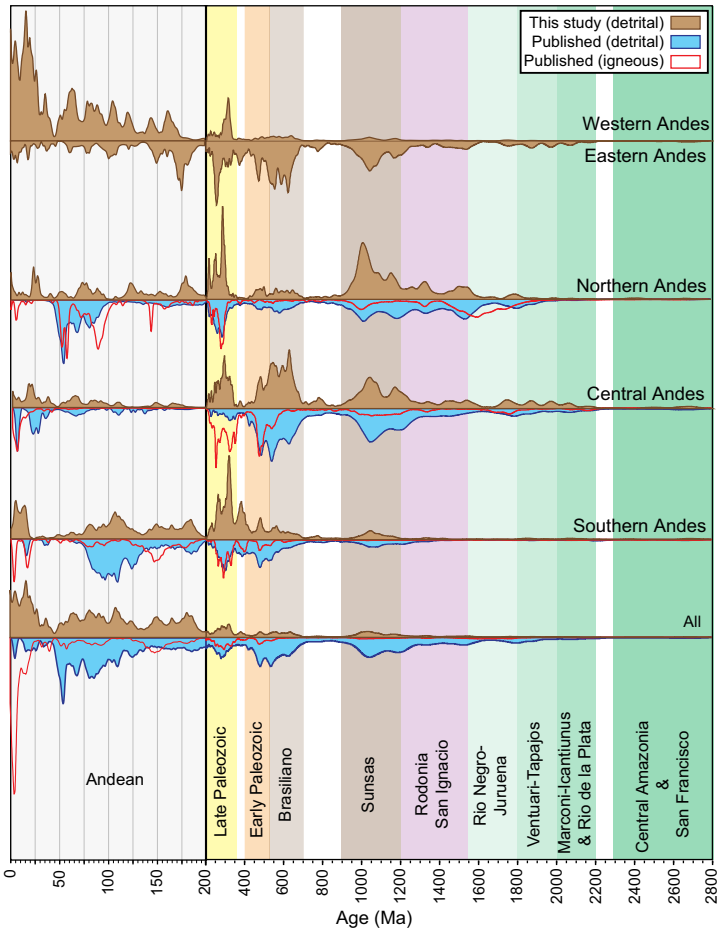

Figure 5. Comparison of U-Pb age distributions from this study, from published analyses of detrital minerals (Supplemental Data 7 [see footnote 8] and Supplemental Item 2 [see footnote 9]), and from published analyses of igneous rocks (Supplemental Data 8 [see footnote 10] and Supplemental Item 3 [see footnote 11]). Ages of basement provinces are from Figure 1. Note that curves have been smoothed with a sliding window average (n = 5) and are normalized according to the number of constituent analyses. The numbers of ages reported are as follows: for this study; published detrital ages; and published igneous ages: northern Andes (NA) = 1339/8871/1492; central Andes (CA) = 2172/12,264/5723; southern Andes (SA) = 2013/5716/2714; all = 5524/26,851/9929.

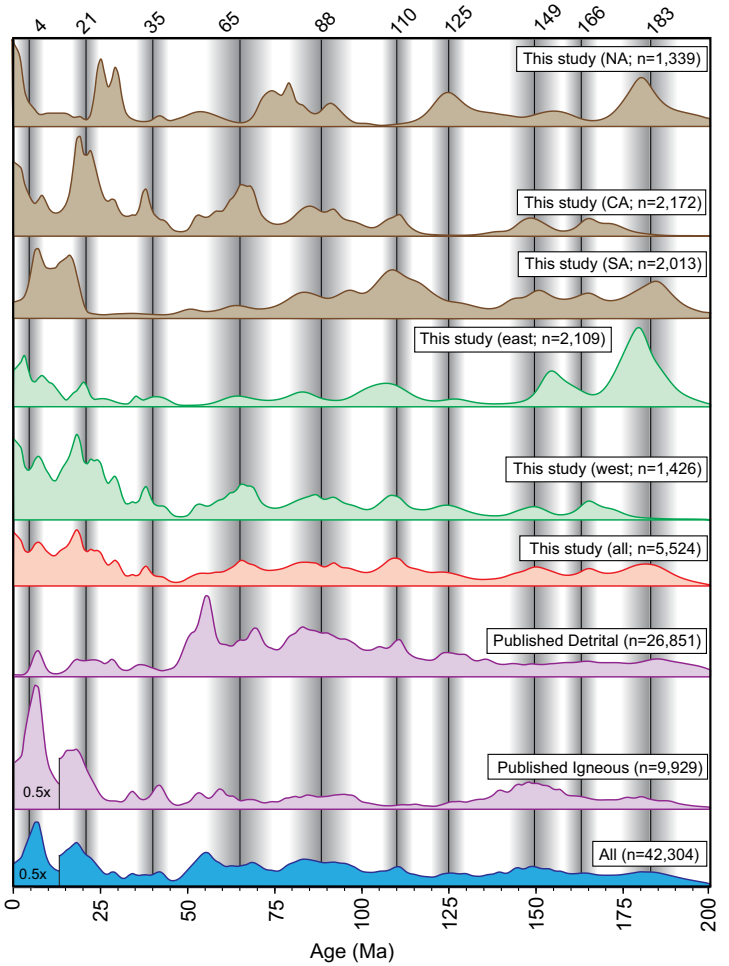

Figure 6. Comparison of 0–200 Ma ages from various data sets. Vertical shaded bands show interpreted maxima of ages based on maximum likelihood analysis of all ages from this study. Note that curves have been smoothed with a sliding window average (n = 5) and are normalized according to the number of constituent analyses.

and temporal focus of the constituent studies. This is apparent in the igneous age distribution (Figs. 5 and 6) by the large proportion of young igneous ages, which reflects the numerous studies of young Andean magmatism. In contrast, previously published detrital ages from sandstones are biased away from these young ages, given that detrital zircons in sandstones always predate deposition. The detrital ages reported herein are biased toward contributions from the modern Andes, given that most large rivers in South America have headwaters in the Andes and that most of our samples were collected from within or adjacent to the Andes. It is also important to note that detrital age distributions may overrepresent older sources given the tendency for zircon grains to be recycled or underrepresent older sources if older grains are too small to be analyzed or are compromised by Pb loss (Gehrels, 2014). For

these reasons, the following discussions focus on general patterns of ages, with the assumption that short-term variations in the proportion of ages may reflect true variations in magmatic addition, whereas variations over longer time periods may be controlled mainly by geologic and/or sampling biases.

Figure 5 shows that there are notable similarities in all three records. Most impressive is the similarity in detrital data sets from this study and previous studies in terms of both presence or absence of ages and proportions of ages. Igneous ages are also similar for most areas and time periods but, as noted above, emphasize young Andean magmatism.

One of the first-order patterns apparent in all data sets is the relatively low abundance of pre–1.2 Ga ages, in spite of the fact that much of South America is underlain by Archean and Paleoproterozoic cratonal rocks (Fig. 1). This low abundance is due in part to biases in sampling (as noted above) and also documents the scarcity of Archean–Paleoproterozoic crystalline rocks in the modern Andes.

The oldest dominant age group includes 1.2–1.0 Ga grains, at least for the central and northern Andes (Fig. 5). These 1.2–1.0 Ga grains presumably record magmatism within the Sunsas belt (Fig. 1), which is exposed along the eastern flank of the northern and central Andes. Grains of these ages may also have been distributed widely across South America during Mesoproterozoic tectonism, as has been documented for sediment derived from the Grenville orogen in North America (e.g., Rainbird et al., 2012).

The next main phase of magmatism recorded in the three data sets begins at ca. 700 Ma and extends into early Paleozoic time (Fig. 5). This magmatism occurred within the Brasiliano belt (0.7–0.5 Ga) during assembly of the South American craton, which coincides with the Pan-African orogeny and the assembly of Gondwana (Windley, 1995; Brito Neves et al., 1999). This phase of continental assembly overlapped with the late Neoproterozoic onset of magmatism along the western margin of South America in a broad and long-lived accretionary orogen (Coney, 1992; Bahlburg and Hervé, 1997; Cawood, 2005; Cawood and Buchan, 2007). Igneous geochronology records magmatism along this convergent margin from ca. 610 Ma until ca. 470 Ma (Cawood and Buchan, 2007), which is also reflected in the record of detrital-zircon ages (Fig. 5).

Our three geochronologic records all show a decrease in magmatism during mid-Paleozoic time (ca. 400 to ca. 360 Ma), followed by significant magmatic addition between 360 and 200 Ma (Fig. 5). This pattern is quite similar to the magmatic history described by Bahlburg and Hervé (1997) and extended through the proto-Andes and to other portions of the Terra Australis orogen by Cawood and Buchan (2007).

The data provide a rich record of variations in magmatism during the past ~200 m.y. As summarized on Figure 6, the record is somewhat different from east to west, from north to south, and in the three different data sets. As a starting point for discussion, we interpret the maxima in ages generated during this study ("This study (all)" on Fig. 6) to indicate times of higher magmatic addition, and we use maximum likelihood analysis to determine midpoints, ranges, and relative proportions (in percent) of magmatism at 183 ± 11 (9% of <200 Ma grains), 166 ± 10 (5%), 149 ± 9 (6%), 125 ± 18 (5%), 110 ± 9 (8%), 88 ± 7 (14%), 65 ± 6 (13%), 35 ± 5 (7%), 21 ± 6 (17%), and 4 ± 4 (16%) Ma (2σ). The shaded gray bars of Figure 6 correspond to these age ranges and midpoints and allow comparison of this interpreted record with other published age distributions and with specific records for NA, CA, SA, and western versus eastern portions of the Andes.

Temporal variations in age abundance in each of the different records shown in Figure 6 suggest that Andean magmatism is strongly cyclic. The period of this cyclicity can be interpreted from the times of higher magmatic addition noted above, which yields an average of ~20 m.y. (10 maxima during 200 m.y.). The periodicity of this cyclicity is quantified with a Lomb-Scargle least-squares spectral analysis. As shown in Figure 7, the record of all previously published and new analyses has the highest signal power (dominant frequency) at ~33 m.y., whereas each of the separate age records has the highest signal power between ~20 and ~34 m.y. Plate convergence velocities along the Andean margin have the highest power at ~20 m.y. Possibilities for the origin of the apparent cyclicity in magmatism are explored below.

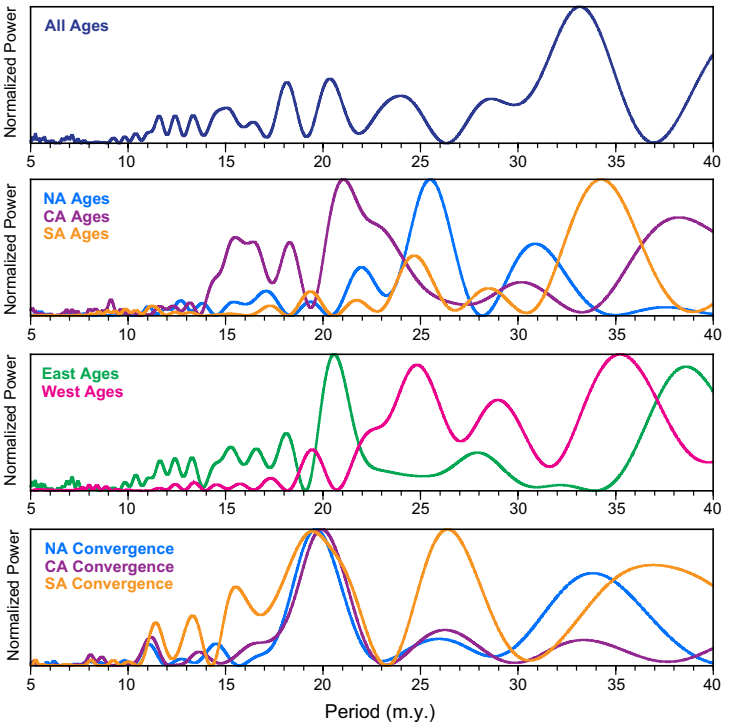

Figure 7. Normalized Lomb-Scargle periodograms of all available data (upper curve), our new ages divided north-south and east-west (middle curves), and relative plate convergence rates for northern Andes (NA), central Andes (CA), and southern Andes (SA) (lower curves). Age distributions have been smoothed with a sliding window average of the closest five ages. Curves were generated with the generic mapping tool (GMT) of Wessel et al. (2013).

Crustal Evolution

The Hf data presented herein, combined with previously published Hf isotope analyses, provide new constraints on the crustal evolution of western South America. All of the available data are shown for NA, CA, and SA on Figures 8–10, and together for all areas on Figure 11. Accompanying these Hf isotope plots are age-distribution diagrams for our new data as well as for all available (igneous and detrital) data.

Yellow arrows on these diagrams show interpreted trajectories of Hf evolution (based on least-squares regression of relevant data). Arrows with slopes that are subparallel to average crustal evolution (black arrows) are interpreted to represent successive remelting of a relatively uniform suite of crustal materials. Arrays that project toward more positive (or less negative) values than average crust (black arrows) are interpreted to record a progressive increase in the proportion of juvenile magmas or slightly older juvenile crust. Arrays that project toward less positive (more negative) values than average crust (black arrows) may result from increased incorporation of old crustal material, involvement of increasingly negative crustal material, and/or reduced involvement of juvenile magmas or crust. Vertical arrays are interpreted to result from melting of crustal materials with highly variable epsilon Hf, along with possible incorporation of juvenile magmas.

Using this interpretive framework as a guide, the available U-Pb/Hf data support the following history of crustal genesis and reworking for western South America:

1. Grains that are >1.6 Ga in age are scarce (especially in NA), and εHf_t values are highly variable, but there is a general trend toward more negative εHf_t values with time. This is interpreted to record Paleoproterozoic

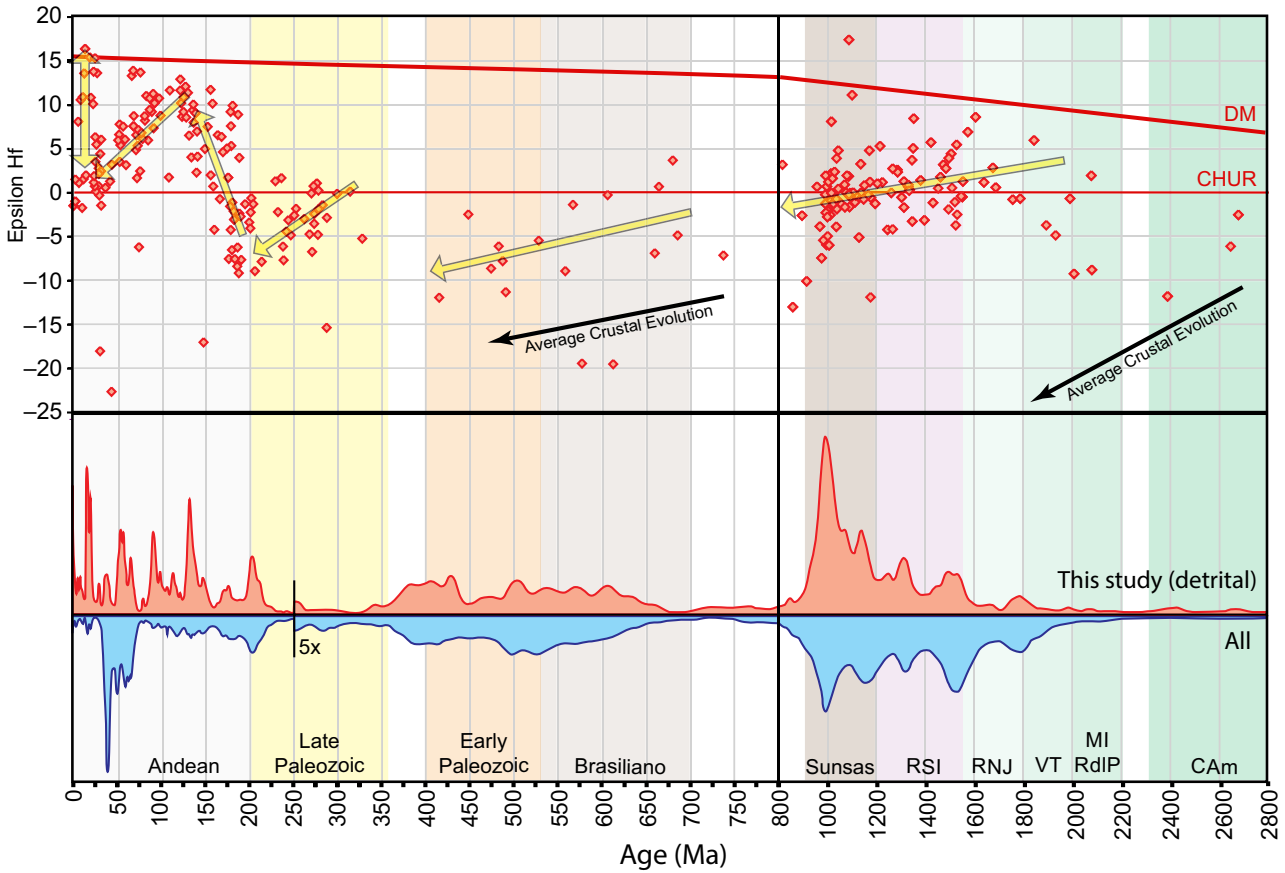

Figure 8. Summary of all available U-Pb and Hf isotope data from northern Andes (NA). See Figure 2 for explanation. All Hf data are from this study (n = 308). U-Pb data are from this study (n = 1340) and from previous studies (Supplemental Data 7 [see footnote 8]; Supplemental Item 2 [see footnote 9]; detrital n = 8871, igneous n = 1492). Note that proportions of >250 Ma ages are enhanced by a factor of 5 relative to <250 Ma ages. Yellow arrows have been determined by least-squares regression of all data within the selected age range. Abbreviations: CAm—Central Amazon craton; CHUR—chondritic uniform reservoir; RdlP—Rio de la Plata craton; DM—depleted mantle array; MI—Maroni-Itacaiunas province; RNJ—Rio Negro Juruena mobile belt; RSI—Rondonian San Ignacio province; VT—Ventuari-Tapajos province.

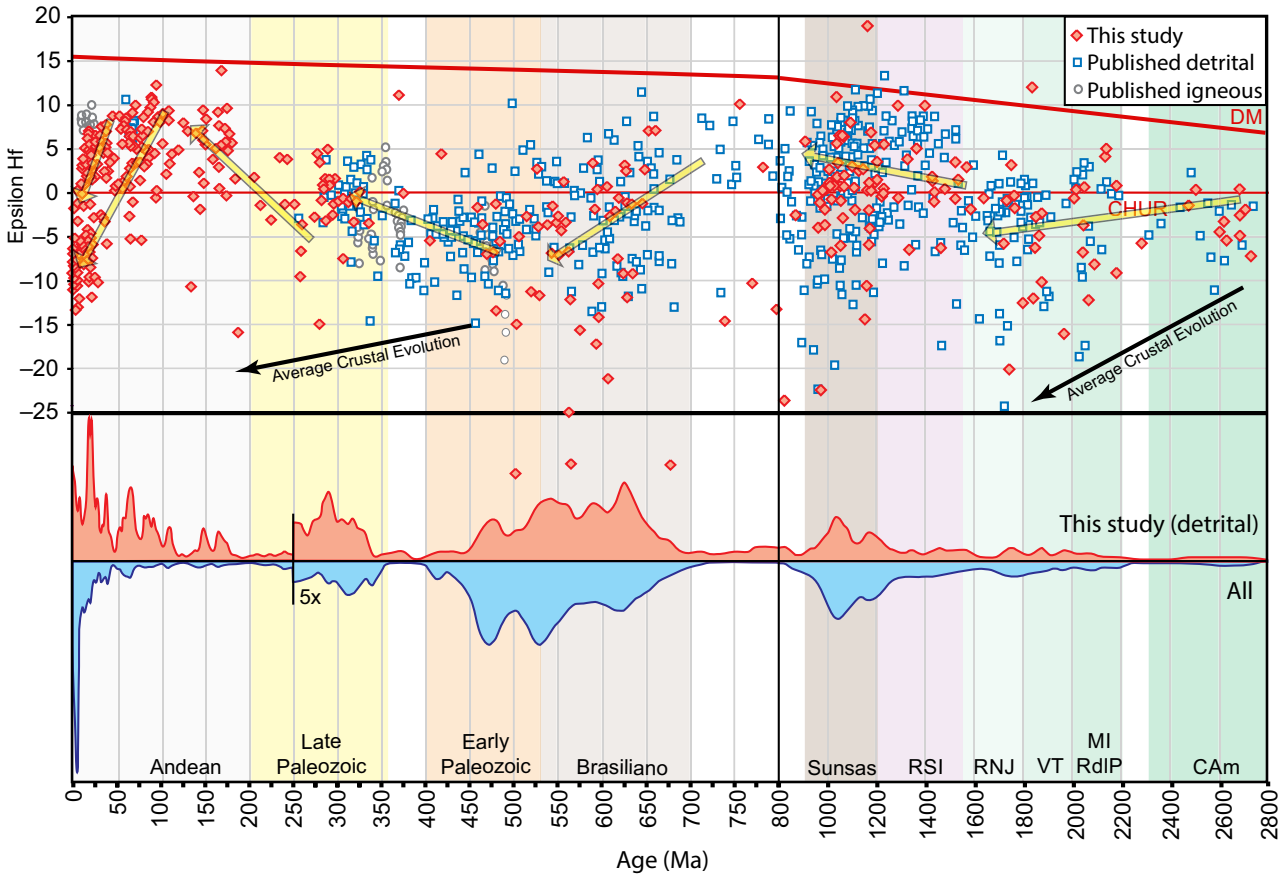

Figure 9. Summary of all available U-Pb and Hf isotope data from central Andes (CA). See Figure 2 for explanation. Hafnium data are from this study (n = 447) and from previous studies (n = 688). Uranium-lead data are from this study (n = 2172) and from the previous studies (Supplemental Data 7 [see footnote 8]; Supplemental Item 2 [see footnote 9]; detrital n = 12,264, igneous n = 5723). Note that proportions of >250 Ma ages are enhanced by a factor of 5 relative to <250 Ma ages. Abbreviations: CAm—Central Amazon craton; CHUR—chondritic uniform reservoir; RdlP—Rio de la Plata craton; DM—depleted mantle array; MI—Maroni-Itacaiunas province; RNJ—Rio Negro Juruena mobile belt; RSI—Rondonian San Ignacio province; VT—Ventuari-Tapajos province.

reworking of mostly Archean crustal materials. There are also numerous grains (especially in CA) with intermediate εHf_t values that include Paleoproterozoic juvenile material. This history pertains mainly to the cratonal rocks of South America (Fig. 1).

2. Between ca. 1.6 Ga and ca. 1.0 Ga, εHf_t values in CA and possibly SA tend to become more positive, reflecting progressive incorporation of juvenile magmas. In contrast, εHf_t values in NA remain intermediate in value, reflecting lesser addition of juvenile crustal material. Given the proximity of the Sunsas belt with NA, the latter history may be relevant for the Mesoproterozoic crustal evolution of northwestern South America. In contrast, the more juvenile Mesoproterozoic zircons in CA and SA may have been shed from other regions of Rodinia—for example, North America, which yields positive εHf_t values for grains of this age (Gehrels and Pecha, 2014). Distribution of these zircons may have occurred as part of a global sediment dispersal system during assembly of Rodinia (e.g., Rainbird et al., 2012) or less likely, from early Paleozoic arrival of North American tectonic fragments with 1.2–1.0 Ga basement (e.g., Cuyania) along the Andean margin (e.g., Astini and Thomas, 1999; Ramos, 2004; Thomas et al., 2004).
3. Between ca. 1.0 Ga and ca. 500 Ma, εHf_t values have trajectories that are generally similar to average crustal evolution (Figs. 8–11). This is interpreted to reflect mainly reworking of >1.0 Ga crustal materials, with little addition of juvenile magma. Franz et al. (2006), Willner et al. (2008), and Bahlburg et al. (2009, 2011) presented a similar conclusion on the basis of Sr, Nd, and Hf isotope signatures of igneous and sedimentary rocks from the central Andes. In addition to this overall trend, there are apparent pull-downs (negative excursions) in εHf_t at 650–550 and ca. 500 Ma (Fig. 11). The older of these excursions likely reflects reworking of older crustal components in Brasiliano orogens, whereas the younger

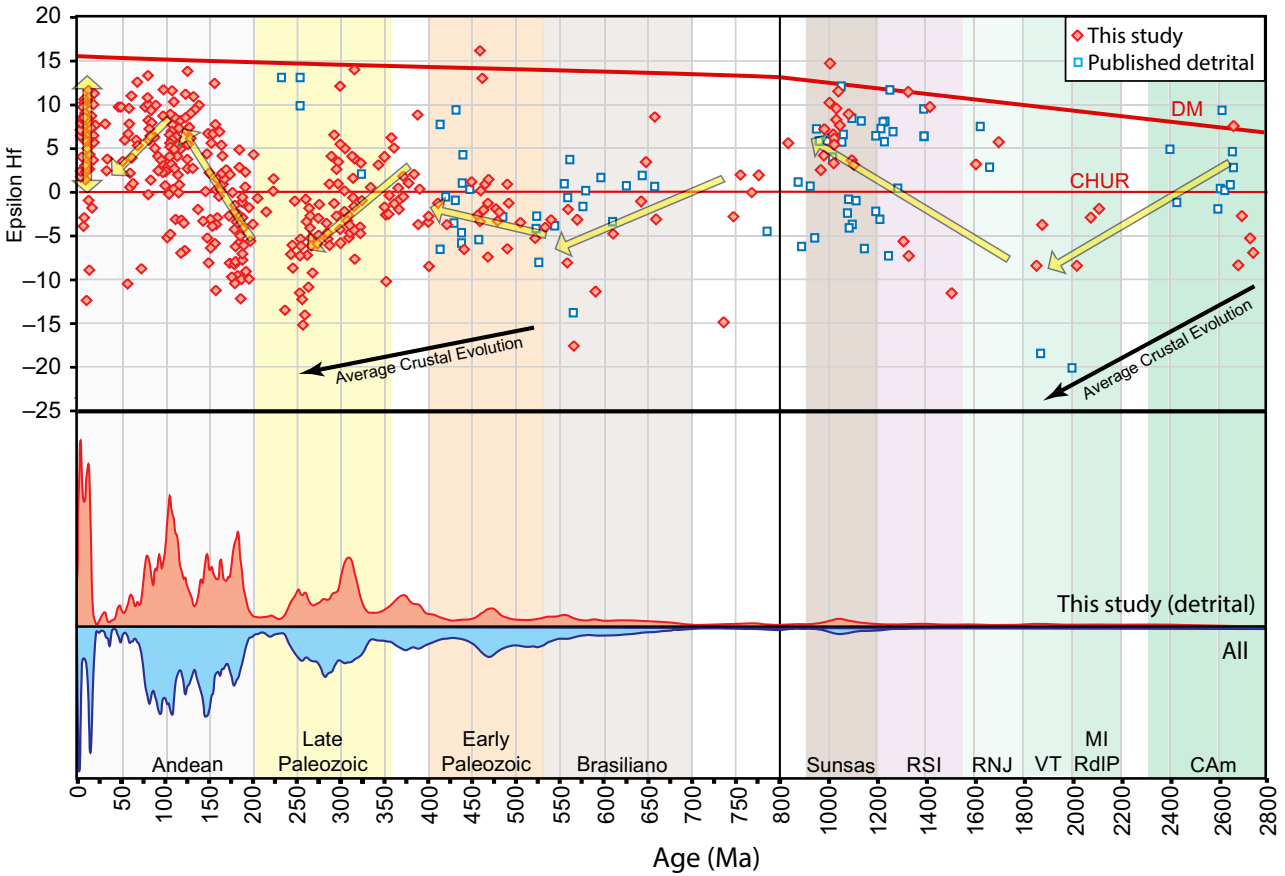

Figure 10. Summary of all available U-Pb and Hf isotope data from southern Andes (SA). See Figure 2 for explanation. Hafnium data are from this study (n = 444) and from previous studies (n = 85). Uranium-lead data are from this study (n = 2013) and from previous studies (Supplemental Data 7 [see footnote 8]; Supplemental Item 2 [see footnote 9]; detrital n = 5716, igneous n = 2714). Note that proportions of >250 Ma ages are enhanced by a factor of 5 relative to <250 Ma ages. Abbreviations: CAm—Central Amazon craton; CHUR—chondritic uniform reservoir; RdlP—Rio de la Plata craton; DM—depleted mantle array; MI—Maroni-Itacaiunas province; RNJ—Rio Negro Juruena mobile belt; RSI—Rondonian San Ignacio province; VT—Ventuari-Tapajos province.

excursion may record involvement of older crustal components within early Paleozoic arcs along the proto-Andean margin (blue dashed lines on Fig. 1). It is interesting that other portions of the broad Terra Australis orogen are also characterized by significant reworking of older crustal materials during this time period (e.g., Cawood et al., 2009, 2012; Kemp et al., 2009; Hawkesworth et al., 2010).

4. Early Paleozoic (500–400 Ma) magmatism yields εHf_t values that remain intermediate or become slightly more positive in the CA and SA. This positive deviation from average crustal evolution suggests that the widespread early Paleozoic magmatism along the Andean margin (e.g., Rapela et al., 1992; Bahlburg and Hervé, 1997; Pankhurst et al., 1998; Coira et al., 1999; Ducea et al., 2010; Einhorn et al., 2015) may have occurred in an overall extensional tectonic regime with thinned continental crust and significant additions of mantle-derived melt (e.g., Ducea et al., 2015).
5. Late Paleozoic (ca. 360 to ca. 250 Ma) magmatism is treated separately from early Paleozoic igneous activity because of the 400–360 m.y. magmatic lull and a significant change in Hf isotope evolution. As shown on Figure 11, there is an overall trend toward more negative εHf_t values during this time, reflecting increased involvement of older crustal materials in late Paleozoic magmatic arcs established along the Andean margin (green dashed lines on Fig. 1). This trend is apparent in NA (Fig. 8) and SA (Fig. 10) but less obvious in the data from CA (Fig. 9). Involvement of continental material may have increased as the late Paleozoic arcs approached and were firmly accreted to the proto-Andean margin (e.g., Willner et al., 2008; Bahlburg et al., 2009; Ramos, 2009).
6. Between ca. 250 and ca. 100 Ma, εHf_t values become more positive in all areas (Figs. 8–11) and mirror the presence of juvenile Sr-Nd-Pb isotopes in rocks of the central Andes (Franz et al., 2006) and epsilon Nd values

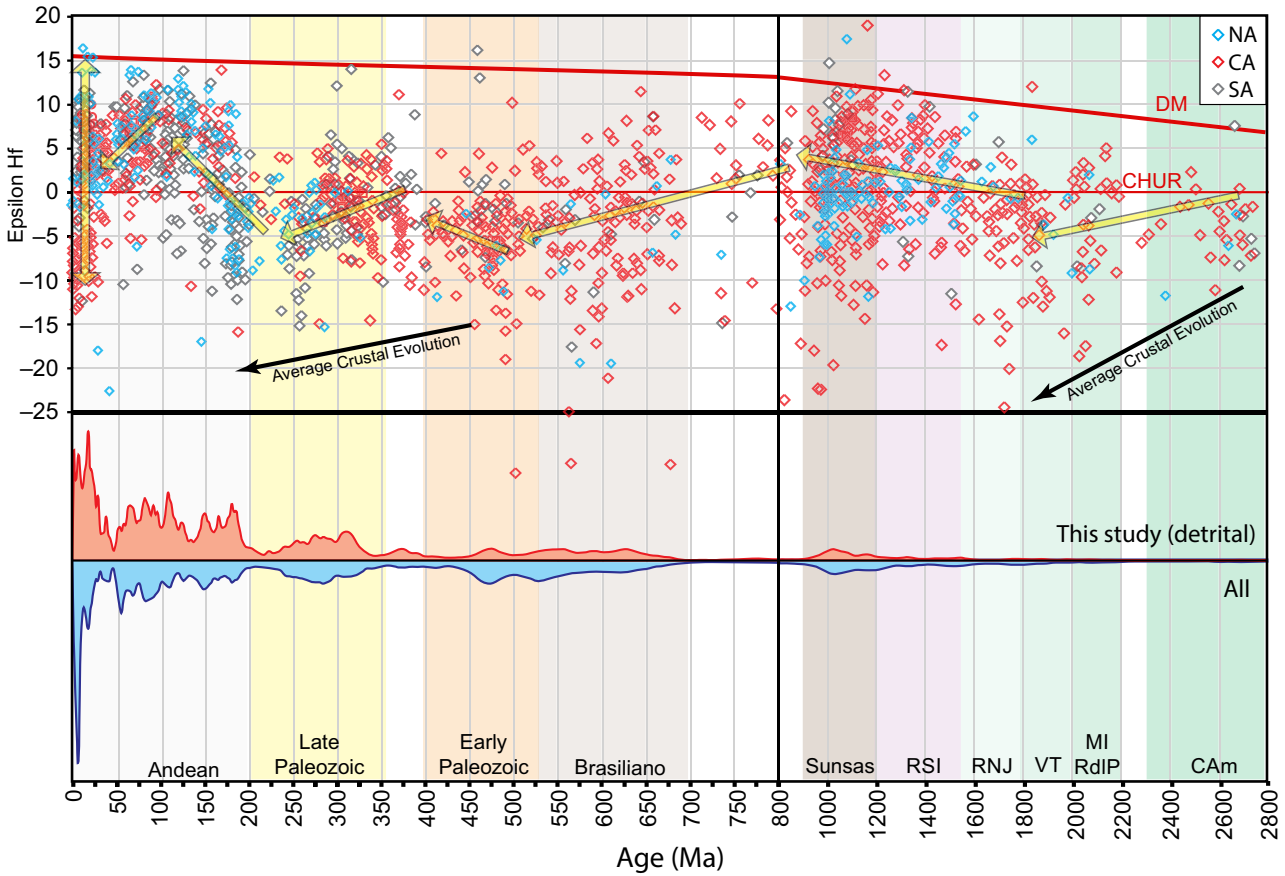

Figure 11. Summary of all available U-Pb and Hf isotope data from South America. See Figure 2 for explanation. Hafnium data are from this study (n = 1199) and from previous studies (n = 436). Uranium-lead data are from this study (n = 5524) and from the previous studies (Supplemental Data 7 [see footnote 8]; Supplemental Item 2 [see footnote 9]; detrital n = 26,851, igneous n = 9929). Abbreviations: CAm—Central Amazon craton; CHUR—chondritic uniform reservoir; RdlP—Rio de la Plata craton; DM—depleted mantle array; MI—Maroni-Itacaiunas province; RNJ—Rio Negro Juruena mobile belt; RSI—Rondonian San Ignacio province; VT—Ventuari-Tapajos province.

in Patagonia (Hervé et al., 2007). This trend is interpreted to result in large part from Triassic through Early Cretaceous extensional tectonism in the subduction system that is well documented all along the Andean margin (Fig. 12; Franz et al., 2006; Ramos, 2009; Maloney et al., 2013; Rossel et al., 2013). Such extension is also manifest as widespread rift-related strata and normal faults of Triassic and Jurassic age (Ramos, 2009), formation of the Late Jurassic Rocas Verdes backarc basin in the southern Andes (Dalziel et al., 1974), formation of the Salta rift system during Late Jurassic–Early Cretaceous time (Salfity and Marquillas, 1994), and opening of basalt-floored basins during Late Jurassic–Early Cretaceous time in the northern Andes (Maloney et al., 2013). The observed trend toward more positive εHf_t values may have also resulted from migration of the magmatic arc westward. As reported by Haschke et al. (2002, 2006) and Franz et al. (2006), the Late Jurassic–Early Cretaceous magmatic arc was situated along the far-western margin of the orogen, which is underlain by Paleozoic arc terranes containing little evolved continental material (Fig. 1).

7. Between ca. 100 and ca. 35 Ma, most zircons lie along trends toward more negative εHf_t values that are steeper than average crustal evolution (Figs. 8–11). This is interpreted to reflect a progressive decrease in the proportion of juvenile magma generated within the arc systems and/or reworking of progressively older crustal materials. The former may be related to a change in subduction dynamics caused by an increase in the age of the slab being subducted and/or an increase in the convergence rate between South America and outboard ocean basins (e.g., Maloney et al., 2013). It is also likely that the average age of reworked crustal materials increased with time as the magmatic arc migrated back toward cratonal South America (e.g., Haschke et al., 2002,

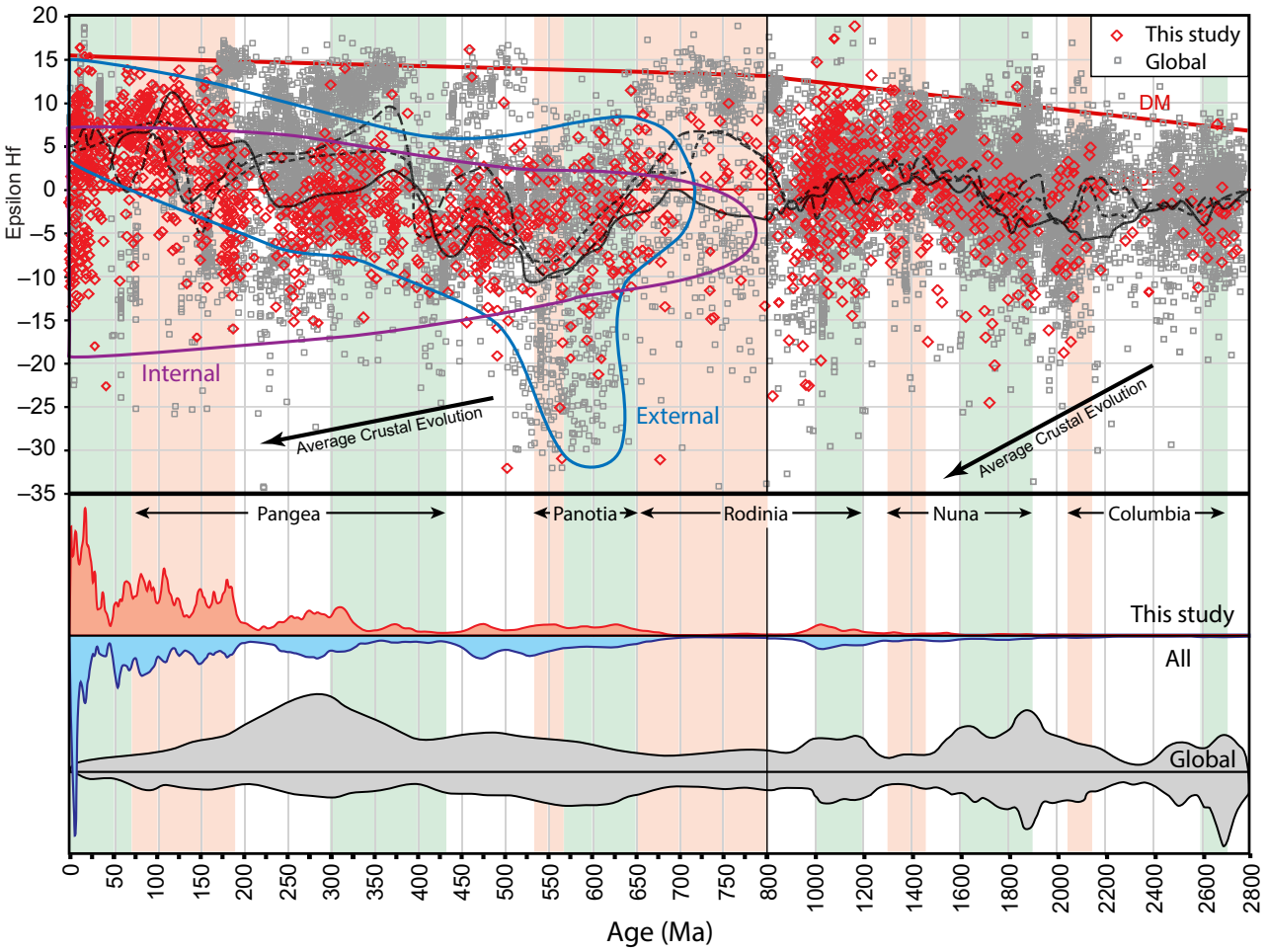

Figure 12. Comparison of U-Pb and Hf isotope data from South America with global compilations of combined zircon U-Pb and Hf isotope data. See Figure 2 for explanation of plot. Hafnium data (upper panel) are from this study (red diamonds; n = 1199) and from the global compilation of Belousova et al. (2010) (n = 12,375; gray squares). Also shown are running mean values from Belousova et al. (2010) with a short dashed line; from Cawood et al. (2012) with a solid line (n = ~7000); and from Condie (2014) with a long dashed line, as well as fields for internal orogens (purple line) and external orogens (blue line) from Collins et al. (2011). Uranium-lead data (lower panel) are from this study (n = 5524), all available data from South America (n = 42,304), and the global compilations of Belousova et al. (2010; n = 23,178) (upper curve) and Condie (2014; n = 37,188) (lower curve). Vertical color bands are from Condie (2014), with green = supercontinent assembly and red = supercontinent breakup.

2006; Franz et al., 2006). Although most zircons lie along this apparent trend, at least in NA and CA, it is important to note that many <100 Ma zircons (especially in SA) yield highly positive εHf_t values. Variations in the proportion of juvenile versus reworked evolved materials are not surprising given the length and complexity of the Andean magmatic arc system.

8. Zircons that are younger than ca. 35 Ma yield highly variable εHf_t values, ranging from –15 to +15 (Fig. 11), which is similar to the broad range of epsilon Nd values in Patagonia (Pankhurst et al., 1999; Hervé et al., 2007). This variation is interpreted to reflect the broad range of tectonic settings along the Andean magmatic arc, from areas of crustal thickening where magmas are forming due to crustal melting, to areas of extension where mantle-derived melts are present (e.g., Kay et al., 2005; DeCelles et al., 2009, 2015; Ramos, 2009).

DISCUSSION

Magmatic Processes

There are relatively consistent patterns of magmatism and crustal evolution in all of the geochronologic and Hf isotopic data sets available for South America. In terms of ages of felsic to intermediate-composition (e.g., zircon-bear-

ing) magmas, the history is apparently episodic, with long-term patterns that parallel the first-order global record (Fig. 12; Voice et al., 2011; Condie, 2014). Significant mismatches are the abundance of <200 Ma ages and the scarcity of >1.4 Ga ages in our South American record, which is not surprising given that most of our samples were collected in proximity to the Andean orogen or from rivers with headwaters in the Andes. This apparent episodicity, with a period of ca. 0.6 Ga, is widely ascribed to aspects of crustal generation and/or preservation associated with the supercontinent cycle (Hawkesworth et al., 2009, 2010; Belousova et al., 2010; Condie et al., 2011; Voice et al., 2011; Condie, 2014), with periods of low zircon production and/or preservation related to breakup of supercontinents (Fig. 12).

As noted above, there is also a strong episodicity in the ages of magmatism during the past 200 m.y. (Figs. 6 and 7). Generally similar times of high and low magmatism are apparent in all data sets, with age maxima at ca. 183, 166, 149, 125, 110, 88, 65, 35, 21, and 4 Ma (shaded gray bars on Fig. 6). There are significant variations in these records, however, with peak ages that are younger, older, or missing entirely along some transects, and the first-order periodicity ranges from ~20 to ~34 m.y. (average of ~33 m.y.) depending on how the data are grouped (Fig. 7).

Possible causes of cyclicity in convergent margin systems have been explored by Davies and Stevenson (1992), Elliott et al. (1997), Haschke et al. (2002, 2006), DeCelles et al. (2009, 2015), Lee and King (2011), Gibert et al. (2012), Ramos et al. (2014), Ducea et al. (2015), and Paterson and Ducea (2015). Explanations generally focus on aspects of the downgoing plate (e.g., convergence velocity, age of downgoing slab, angle of downgoing slab, and dehydration providing fluids for the overlying mantle wedge) versus upper-plate controls such as tectonic thickening and/or thinning and processes of delamination. These recent syntheses have been constructed in large part on the basis of studies by Haschke et al. (2002, 2006) of magmatism in the central Andes, as well as magmatism in western North America.

Haschke et al. (2002, 2006) reported that the central Andes have experienced four phases of magmatism at 195–129, 123–82, 76–37, and 22–0 Ma, yielding an average periodicity of ~50 m.y. (purple fields on Fig. 13). Magmatic gaps are reported to exist at 129–123, 82–76, and 37–22 Ma. Haschke et al. (2002) suggest that a correlation between magma addition and convergence rate may be due to a cycle of decreasing slab dip (periods of high magma addition) followed by slab breakoff or rollback (periods of low magma addition). Ramos (2009) and Ramos et al. (2014) propose an Andean orogenic and/or magmatic cycle

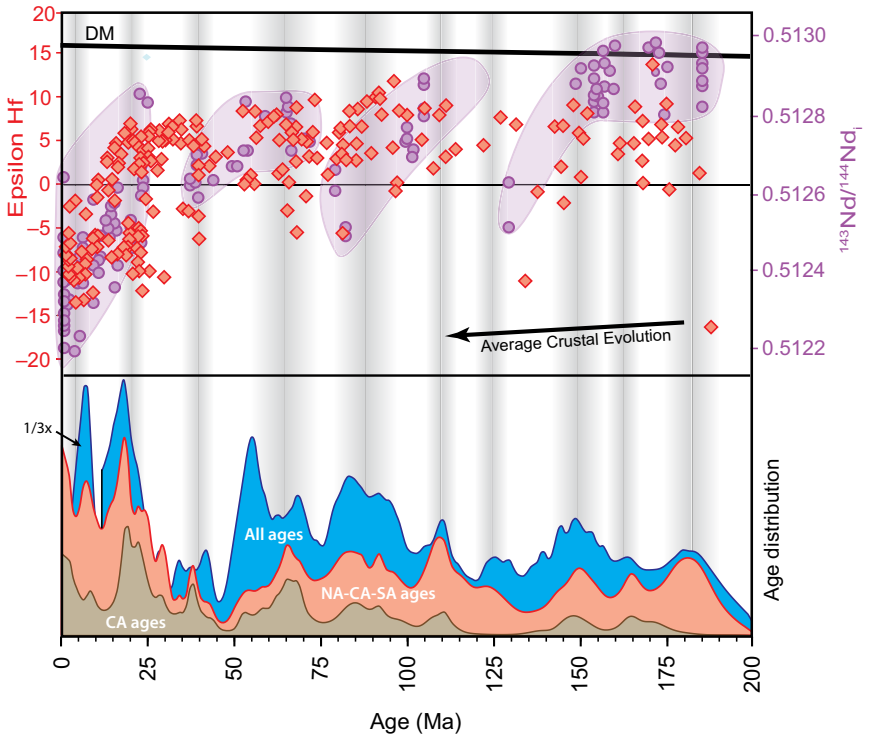

Figure 13. Diagram comparing the results of Haschke et al. (2002) with our central Andes (CA) data for the past 200 m.y. Purple circles and fields in upper plot show age and Nd isotope data of Haschke et al. (2002). Red diamonds in upper plot show CA age and Hf isotope data from this study. Age-distribution diagrams show our results from CA (n = 1339), our new results from all of South America (n = 5524), and all ages available from South America (n = 42,304), all smoothed with a sliding window average of the closest five ages. Vertical gray bands show interpreted age maxima (from Fig. 6). DM—depleted mantle array.

that invokes changes in slab dip and delamination of lower crustal roots as a primary control on types and volumes of magmatism. DeCelles et al. (2009, 2015) provide an alternative explanation of cyclicity that involves periods of compressional tectonism, heating, hydration, eclogitization, and delamination of the upper plate, with less reliance on processes directly associated with the subducting plate (e.g., slab angle and subduction velocity).

Possible tectonic drivers for the cyclicity apparent from our data set are explored on Figure 14, which compares our U-Pb ages and Hf isotope values with convergence velocities (blue lines), rates of absolute westward motion of South America (green lines), and ages of the downgoing slab (purple lines) (from Maloney et al., 2013) for each of our three transects. Of the three parameters, there is little visual evidence of a correlation between magmatic history and either the age of the downgoing plate (purple lines) or the absolute westward motion of South America (green lines). Possible connections between magmatic history and convergence rate between South America and subducting oceanic plates (blue lines) are more difficult to evaluate visually because of the complexity of the various records.

Figure 15 shows the results of our attempts to statistically evaluate possible linkages between magmatism and convergence velocity using continuous wavelet transform (CWT) analysis for the central Andean section (similar results for SA and NA are shown in Supplemental Item 4[12]). Although there appears to be some statistically significant common signal power with a periodicity between 16 and 24 m.y. (Figs. 15C–15E), the signals are inconsistently out of phase (not phase locked) across these periods (e.g., black arrows change direction for same period in Fig. 15E). This indicates that the time lag between the two signals with common power is changing with time. If there were a simple cause and effect relationship between magmatism and plate convergence rates (e.g., a plate convergence rate increases X m.y. before an age distribution increases), we would expect the phases to be locked (e.g., all black arrows pointing in the same direction for the same period in Fig. 15E). This interpretation is further supported by the lack of coherence between the two time series, where only two small areas centered at 20 and 40 Ma (period of ~5 m.y.) show any statistically significant correlation (Fig. 15F). A similar lack of statistically significant correlation is observed for the southern and northern Andean sections (Supplemental Item 4 [see footnote 12]). Additionally, spectral analysis of the convergence velocities (from Maloney et al., 2013) yields highest signal power at ~20 m.y. for all three regions (Fig. 7), which is somewhat shorter than the observed magmatic periodicities. We therefore conclude that the observed magmatic periodicities are not attributable to a simple genetic connection with plate convergence rates.

Crustal Generation and Reworking

As with magmatic processes, our data set provides new insights into processes of crustal generation, reworking, and preservation that operate at two different time scales. On a broader time scale, our data provide an interesting comparison with the Hf isotopic results presented by Belousova et al. (2010),

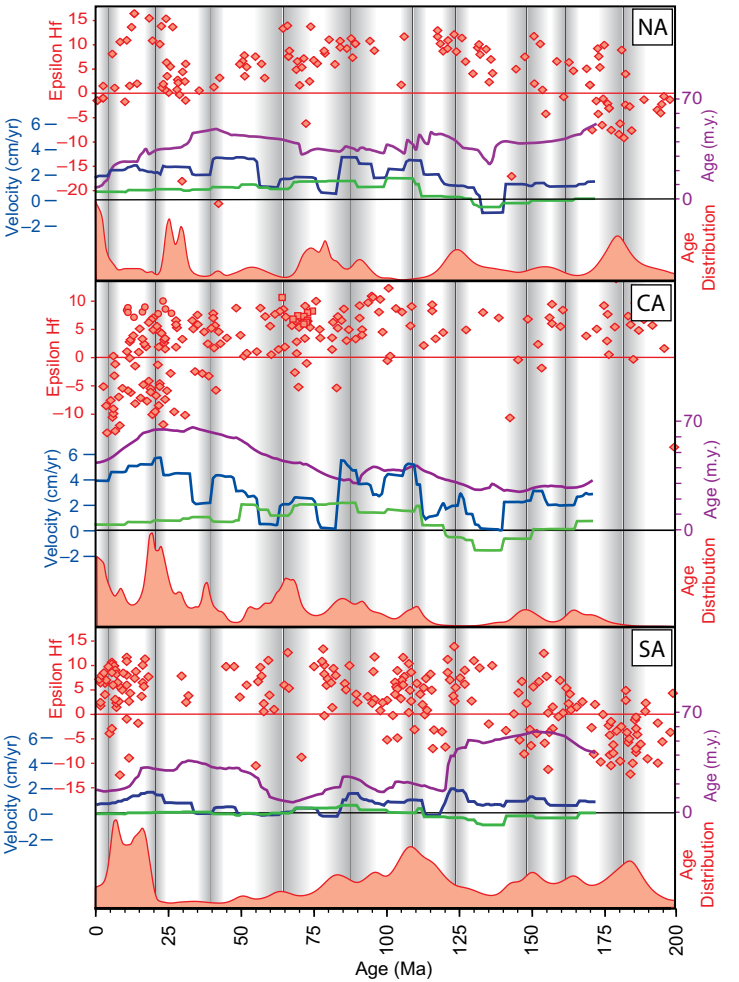

Figure 14. Diagram comparing the results of Maloney et al. (2013) with our data for all three regions (northern Andes [NA], central Andes [CA], and southern Andes [SA]) for the past 200 m.y. Red diamonds in upper diagram show Hf isotope data from this study. Filled red curves in lower portion of each panel show all available U-Pb ages (smoothed with sliding window average of the closest five ages). Vertical gray bands show interpreted age maxima (from Fig. 6). Central portions of each panel show information about plate motion along the Andean margin (NA = average of sites 2–9 of Maloney et al., 2013; CA = average of sites 12–36 of Maloney et al., 2013; SA = average of sites 39–54 of Maloney et al., 2013). Plate velocities are shown relative to scale on left (in blue), with green lines showing absolute westward velocity of South America and blue lines showing relative convergence velocity between South America and outboard oceanic plates. Purple lines show the age of the downgoing plate, with scale shown on the right (in purple).

Supplemental Item 4 (Continuous Wavelet Transform Analysis)

Magmatic History and Crustal Genesis of Western South America: Constraints from U-Pb ages and Hf Isotopes of Detrital Zircons in Modern Rivers

Martin Pepper, George Gehrels, Alex Pullen, Mauricio Ibanez-Mejia, Kevin M. Ward, and Paul Kapp

Supplemental Item 4: Continuous Wavelet Transform Analysis

In this supplemental item, we provide additional results from our continuous wavelet transform (CWT) analysis of the Northern, Central, and Southern Andean sections presented in the main text as well as a brief description of CWT analysis (Figs. S1-S4). Traditional Fourier analysis implicitly assumes any physical relationships are stationary in time. The wavelet method employed in our analysis has several advantages over traditional Fourier analysis and is particularly well-suited for analyzing geological and geophysical time-series that may exhibit periodic behavior which varies in time with localized intermittent periodicities (Torrence & Compo, 1998). For each individual time-series, we calculate the continuous (local) wavelet power spectrum. Because the wavelet is not everywhere localized in time, we define a cone of influence (COI), where edge effects are significant. We also define a ≥95% confidence interval using a first order autoregressive process (Allen & Smith, 1996) that models red noise (random walk noise) to identify statistically significant areas of signal generated wavelet power. The continuous (local) wavelet power spectrum results for each individual time-series analyzed show signal power at similar periods as the Lomb-Scargle periodograms (Fig. 7) with additional information about localized intermittent periodicities.

[12]Supplemental Item 4. Continuous wavelet transform analysis. Please visit http://dx.doi.org/10.1130/GES01315.S12 or the full-text article on www.gsapubs.org to view the Supplemental Item.

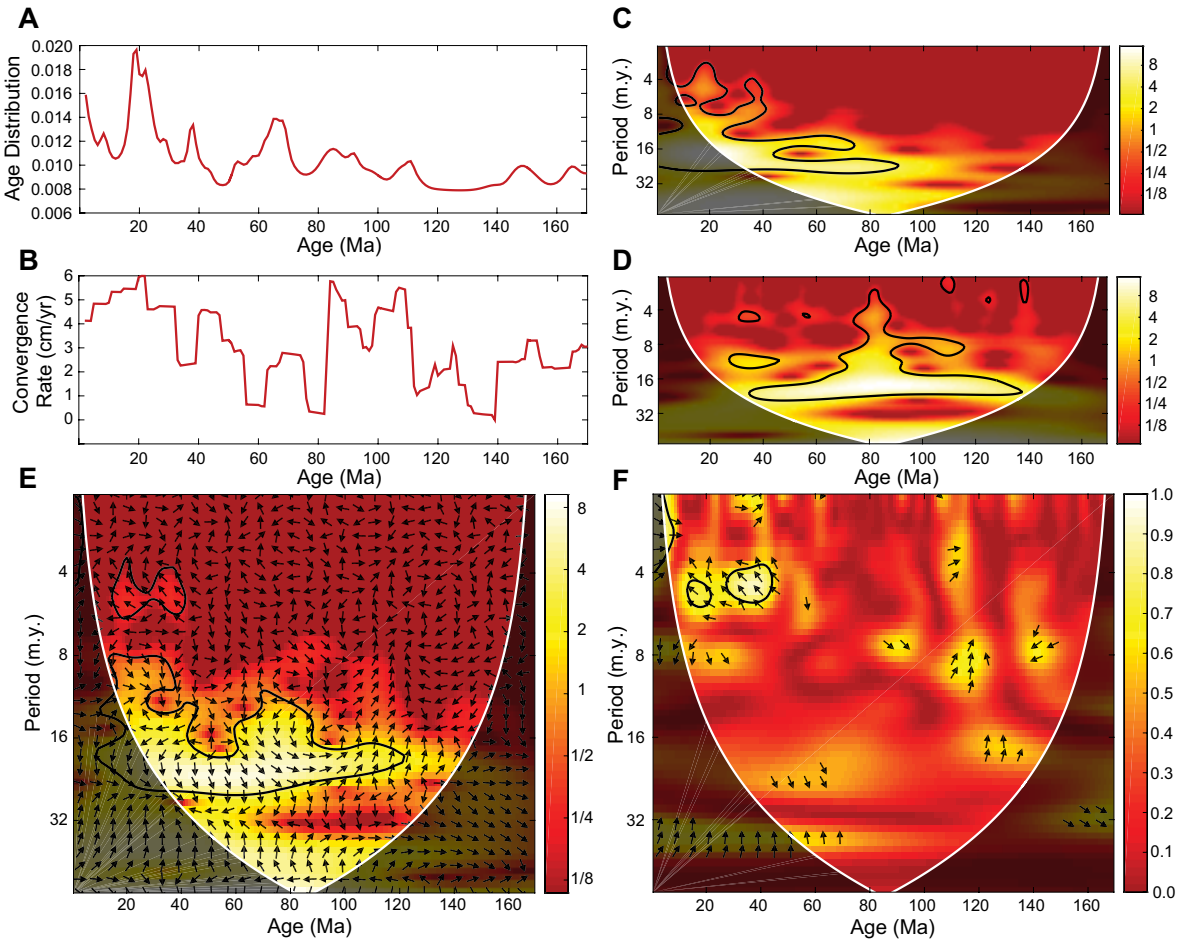

Figure 15. Results of our continuous wavelet transform (CWT) analysis for the central Andean (CA) section. Magmatic history (A) and convergence rate; (B) time series used in CWT analysis, (C and D) continuous wavelet power for the A and B time series; (E) cross wavelet transform of the two time series; and (F) wavelet coherence of the two time series. The ≥95% confidence interval against red noise is shown as a thick white contour. The cone of influence (COI), where edge effects are significant, is shown as a masked dark section. Phase differences are shown as black arrows where in-phase arrows point to the right and anti-phase (180° out-of-phase) arrows point to the left.

Collins et al. (2011), Condie et al. (2011), and Cawood et al. (2012) (Fig. 12). Our data resemble the global patterns prior to ca. 800 Ma but are somewhat different for younger time periods. The first significant difference is the abundance of juvenile values from 800 to 650 Ma in the Belousova et al. (2010) compilation, which is not seen in South America. Next is the negative excursion from 650 to 500 Ma in the global data sets (due largely to Pan-African tectonism), which is not seen in our data set. A final difference is the abundance of juvenile values from 400 to 200 Ma in the Belousova et al. (2010) compilation (mainly due to juvenile terranes of Asia), which is not found in South America. In comparison with the internal versus external orogens recognized by Collins et al. (2011), as expected, our data from South America clearly resemble other external orogens (Fig. 12).

On a more recent time scale, our data record a dramatic change in crustal evolution during the past 200 m.y. that is not seen in older South American orogenic events or in the global record (Figs. 12–14). Magmatism in early Mesozoic magmatic arcs initiated with relatively evolved Hf signatures that reflect significant incorporation of older continental crust. Beginning at ca. 180 Ma, εHf_t values become more juvenile until ca. 100 Ma, and then become slightly more negative until ca. 35 Ma. The pre-100 Ma trend toward more juvenile values may result largely from extension within the magmatic arc, as has been proposed for the Tasmanides (Kemp et al., 2009; Hawkesworth et al., 2010). This excursion to more juvenile values may also have resulted from the Late Jurassic–Early Cretaceous magmatic arc having been located farther to the west, where there was little influence from older continental or continental margin assemblages.

As has been suggested in most previous syntheses (e.g., Haschke et al., 2002, 2006; Kay et al., 2005; DeCelles et al., 2009, 2015; Ramos, 2009; Ramos et al., 2014), the general trend toward more evolved values during the past ~100 m.y. most likely resulted from the onset of shortening and crustal thickening within the Andes, causing more crustal melting, and also migration of magmatism eastward into older crust. The broad range of εHf_t values for <35 Ma zircons, from +15 to –15 (Fig. 11), results from profound variations in tectonic setting along the length of the Andes, with magmatism covering the full range of pure crustal recycling to mainly juvenile input from the mantle. Such a broad range of petrogenetic processes is rare during any time period in Earth history (Fig. 12).

Of particular interest for this study are the La/Yb, Sr isotope, and Nd isotope patterns reported by Haschke et al. (2002, 2006), which were interpreted to record changes in Andean subduction dynamics on a ~50 m.y. time scale. As shown on Figure 13, the patterns appear to record increasing incorporation of crustal material toward the end of each cycle, as well as an overall trend toward more evolved values during the past 200 m.y. The data generated and compiled in this study from the same region (CA) show the general trend toward more evolved values, especially since ca. 100 Ma. However, the separate ~50 m.y. pull-downs apparent from the Nd, Sr, and La/Yb data are not apparent in our Hf-in-zircon data set, and, as noted above and shown on Figure 13, our age data do not record the magmatic gaps interpreted by Haschke et al. (2002) to separate the magmatic cycles. A possible explanation of these discrepancies is that our record is dominated by felsic to intermediate composition magmatism, whereas the samples reported by Haschke et al. (2002) also include mafic components.

CONCLUSIONS

This study of U-Pb geochronology and Hf isotope geochemistry yields five major contributions to understanding the magmatic history and crustal evolution of western South America:

1. Our U-Pb ages (n = 5524), combined with previously published ages (n = 36,764), record phases of high magmatic addition at 1.6–0.9 Ga, 700–400 Ma, 360–200 Ma, and 190 Ma to the present day (Fig. 12). Because this record has been assembled largely from studies of detrital zircons in rivers with headwaters in the modern Andes, the age distributions are biased toward felsic to intermediate composition magmatism, and toward younger events that are preserved in the Andean orogen.
2. Magmatism during the past 200 m.y. has been variable north-to-south along the length of the Andes and east-west across the Andes, and igneous rocks versus detrital minerals yield slightly different patterns (Fig. 6). Most records are consistent, however, with age maxima at 183 (±11), 166 (±10), 149 (±9), 125 (±18), 110 (±9), 88 (±7), 65 (±6), 35 (±5), 21 (±6), and 4 (±4) Ma (2σ) (shaded gray bars on Fig. 6). Magmatic records for NA, CA, and SA have periodicities that range from ~20 to ~34 m.y. (Fig. 7). Although convergence rates between the South America and Pacific and Nazca oceanic plates have a somewhat similar periodicity of ~20 m.y. (Maloney et al., 2013; Fig. 14), continuous wavelet transform analysis indicates that there is no temporal connection between magmatism and convergence rate (Fig. 15).
3. The distribution of all ages from western South America has significant overlap with global age distributions, which are widely interpreted to record processes of crustal generation and/or preservation related to the supercontinent cycle (Hawkesworth et al., 2009, 2010; Belousova et al., 2010; Condie et al., 2011; Voice et al., 2011; Cawood et al., 2012; Condie, 2014). The main differences are the lesser abundance of >1.2 Ga ages and greater abundance of <200 Ma ages (Fig. 12) in our western South American record.
4. Our Hf isotope determinations (n = 1199), combined with published Hf isotope data (n = 813), record eight phases in the crustal evolution of western South America (Fig. 11):
   - Prior to ca. 1.6 Ga, most grains record Paleoproterozoic reworking of older Archean crustal materials.
   - Between ca. 1.6 Ga and ca. 1.0 Ga, an increasing proportion of juvenile magma was mixed with reworked Paleoproterozoic–Archean crust.
   - Between ca. 1.0 Ga and ca. 500 Ma, most magmatic processes involved reworking of older crustal materials, with little generation of new crust.
   - Between ca. 500 and 400 Ma, increasing juvenile magmatism in CA resulted from extension and crustal thinning throughout the Famatina and related magmatic arcs (e.g., Ducea et al., 2015).
   - Following a magmatic lull between ca. 400 and ca. 360 Ma, there was significant juvenile magmatism in proto-Andean arc terranes, followed by a trend toward greater interaction with older crust until ca. 250 Ma. This increase in crustal reworking is presumably related to accretion and/or consolidation of oceanic arc terranes along the Andean margin.
   - Following a magmatic lull between ca. 240 and ca. 180 Ma, and continuing until ca. 100 Ma, magmatism increased, and significant volumes of juvenile magma were generated. This phase coincides with extensional tectonism (Ramos, 2009), a reduction in both convergence velocity and westward motion of South America (Maloney et al., 2013), and migration of the magmatic arc westward into more juvenile arc-type crust (e.g., Franz et al., 2006).
   - Between ca. 100 Ma and ca. 35 Ma, abundant magmatism continued, but with decreasing juvenile magma and increasing involvement of older continental crust. This phase presumably relates to contractional tectonism and initiation of uplift of the modern Andes (Kay et al., 2005; Franz et al., 2006; Ramos, 2009; DeCelles et al., 2015), an increase in both convergence velocity and westward motion of South America (Maloney et al., 2013), and migration of the magmatic arc eastward into more evolved crust (Haschke et al., 2002, 2006; Franz et al., 2006).
   - During the past ~35 m.y., high-addition-rate magmatism continued with highly variable Hf isotope signatures. No evolutionary trends are apparent; although there is a spatial variation with more juvenile values in the northern and southern Andes and more evolved values in

the central Andes (Figs. 11 and 14). These variations presumably reflect differing tectonic settings (contractional versus extensional) along and across the orogen in response to changes in both the subducting and overriding plates.

5. The South American record of crustal evolution is quite similar to the global record (e.g., Belousova et al., 2010; Cawood et al., 2012; Condie, 2014), except that western South America lacks significant volumes of 800–650 Ma and 400–200 Ma juvenile crust and highly evolved 650–500 Ma crust (Fig. 12). The overall trend toward more juvenile magmatism is similar, however, to other external orogens of the world (Collins et al., 2011). The main pattern of increasing juvenile magmatism from 200 to 100 Ma and decreasing juvenile magmatism after 100 Ma (Fig. 12) may result from Jura-Cretaceous extension within and behind the Andean magmatic arc system, as well as migration of the magmatic arc first outboard into more juvenile arc terranes and then inboard into crust with greater proportions of older continental crust.

ACKNOWLEDGMENTS

We are grateful for support from the Geological Society of America (student grant 9157-06) and the Chevron-Texaco summer support grant awarded to M. Pepper. Analyses were conducted in the Arizona LaserChron Center, which is supported by National Science Foundation grant EAR-1338583. We also thank LaserChron staff members Chen Li, Gayland Simpson, Chelsi White, Dominique Geisler, Mark Pecha, Clayton Loehn, and Glynis Jehle for assistance with sample preparation and analysis. Ned Brown provided valuable discussions of the work presented in this publication, and David Meko and Susan Beck provided assistance with our statistical analyses. We would also like to thank the ExxonMobil Convergent Orogenic Systems Analysis (COSA) project, which provided many discussions and covered costs of a central Andean field trip. We also thank Agustin Cardona, Franco Urbani, David Mendi, Camilo Bustamante, Giovani Jimenez, and Herman Bayona for assistance with sample collection during this project. A very thorough and insightful review was provided by H. Bahlburg.

REFERENCES CITED

Aceñolaza, F.G., Miller, H., and Toselli, A.J., 2002, Proterozoic–early Paleozoic evolution in western South America—A discussion: Tectonophysics, v. 354, p. 121–137, doi:10.1016/S0040-1951(02)00295-0.

Allen, M.R., and Smith, L.A., 1996, Monte Carlo SSA: Detecting irregular oscillations in the presence of coloured noise: Journal of Climate, v. 9, p. 3373–3404, doi:10.1175/1520-0442(1996)009<3373:MCSDIO>2.0.CO;2.

Allmendinger, R.W., Jordan, T.E., Kay, S.M., and Isacks, B.L., 1997, The evolution of the Altiplano-Puna Plateau of the Central Andes: Annual Review of Earth and Planetary Sciences, v. 25, p. 139–174, doi:10.1146/annurev.earth.25.1.139.

Amelin, Y., and Davis, W.J., 2005, Geochemical test for branching decay of ^{176}Lu: Geochimica et Cosmochimica Acta, v. 69, p. 465–473, doi:10.1016/j.gca.2004.04.028.

Armstrong, R.L., 1968, A model for the evolution of strontium and lead isotopes in a dynamic earth: Reviews of Geophysics, v. 6, p. 175–199, doi:10.1029/RG006i002p00175.

Aspden, J.A., and McCourt, W.J., 1986, Mesozoic oceanic terrane in the central Andes of Colombia: Geology, v. 14, p. 415–418, doi:10.1130/0091-7613(1986)14 <415:MOTITC>2.0.CO;2.

Aspden, J.A., McCourt, W.J., and Brook, M., 1987, Geometrical control of subduction-related magmatism: The Mesozoic and Cenozoic plutonic history of western Colombia: Journal of the Geological Society of London, v. 144, p. 893–905, doi:10.1144/gsjgs.144.6.0893.

Astini, R.A., and Thomas, W.A., 1999, Origin and evolution of the Precordillera terrane of western Argentina: A drifted Laurentian orphan, *in* Ramos, V.A., and Keppie, J.D., eds., Laurentia Gondwana Connections before Pangea: Geological Society of America Special Paper 336, p. 1–20, doi:10.1130/0-8137-2336-1.1.

Augustsson, C., and Bahlburg, H., 2008, Provenance of late Palaeozoic metasediments of the Patagonian proto-Pacific margin (southernmost Chile and Argentina): International Journal of Earth Sciences, v. 97, p. 71–88, doi:10.1007/s00531-006-0158-7.

Augustsson, C., Muenker, C., Bahlburg, H., and Fanning, C.M., 2006, Provenance of late Palaeozoic metasediments of the SW South American Gondwana margin: A combined U-Pb and Hf-isotope study of single detrital zircons: Journal of the Geological Society of London, v. 163, p. 983–995, doi:10.1144/0016-76492005-149.

Bahlburg, H., and Hervé, F., 1997, Geodynamic evolution and tectonostratigraphic terranes of northwestern Argentina and northern Chile: Geological Society of America Bulletin, v. 109, no. 7, p. 869–884, doi:10.1130/0016-7606(1997)109<0869:GEATTO>2.3.CO;2.

Bahlburg, H., Vervoort, J.D., DuFrane, S.A., Bock, B., Augustsson, C., and Reimann, C., 2009, Timing of crust formation and recycling in accretionary orogens: Insights learned from the western margin of South America: Earth-Science Reviews, v. 97, p. 215–241, doi:10.1016/j.earscirev.2009.10.006.

Bahlburg, H., Vervoort, J.D., DuFrane, S.A., Carlotto, V., Reimann, C., and Cardenas, J., 2011, The U-Pb and Hf isotope evidence of detrital zircons of the Ordovician Ollantaytambo Formation, southern Peru, and the Ordovician provenance and paleogeography of southern Peru and northern Bolivia: Journal of South American Earth Sciences, v. 32, p. 196–209, doi:10.1016/j.jsames.2011.07.002.

Baldwin, M.P., Gray, L., Allmendinger, R.W., Jordan, T.E., Kay, S.M., and Isacks, B.L., 1997, The evolution of the Altiplano-Puna plateau of the Central Andes: Annual Review of Earth and Planetary Sciences, v. 25, p. 139–174, doi:10.1146/annurev.earth.25.1.139.

Barbeau, D.L., Gombosi, D.J., Zahid, K.M., Bizimis, M., Swanson-Hysell, N., Valencia, V., and Gehrels, G.E., 2009, U-Pb zircon constraints on the age and provenance of the Rocas Verdes basin fill, Tierra del Fuego, Argentina: Geochemistry Geophysics Geosystems, v. 10, no. 12, Q12001, doi:10.1029/2009GC002749.

Belousova, E.A., Kostitsyn, Y.A., Griffin, W.L., Begg, G.C., O'Reilly, S.Y., and Pearson, N.J., 2010, The growth of continental crust: Constraints from zircon Hf isotope data: Lithos, v. 119, p. 457–466, doi:10.1016/j.lithos.2010.07.024.

Borrero, C., Pardo, A., Jaramillo, C.M., Osorio, J.A., Cardona, A., Flores, A., Echeverri, S., Rosero, S., García, J., and Castillo, H., 2012, Tectonostratigraphy of the Cenozoic Tumaco forearc basin (Colombian Pacific) and its relationship with the northern Andes orogenic build up: Journal of South American Earth Sciences, v. 39, p. 75–92, doi:10.1016/j.jsames.2012.04.004.

Bouvier, A., Vervoort, J.D., and Patchett, P.J., 2008, The Lu-Hf and Sm-Nd isotopic composition of CHUR: Constraints from unequilibrated chondrites and implications for the bulk composition of terrestrial planets: Earth and Planetary Science Letters, v. 273, p. 48–57, doi:10.1016/j.epsl.2008.06.010.

Brito Neves, B.B.D., Campos Neto, M.D.C., and Fuck, R.A., 1999, From Rodinia to Western Gondwana: An approach to the Brasiliano–Pan African Cycle and orogenic collage: Episodes, v. 22, p. 155–166.

Campbell, I.H., and Allen, C.M., 2008, Formation of supercontinents linked to increases in atmospheric oxygen: Nature Geoscience, v. 1, p. 554–558, doi:10.1038/ngeo259.

Cardona, A., Cordani, U.G., Ruiz, J., Valencia, V.A., Armstrong, R., Nutman, A., and Sanchez, A., 2009, U/Pb zircon and Nd isotopic signatures of the pre-Mesozoic metamorphic basement of the Eastern Peruvian Andes: Growth and Provenance of a Late Neoproterozoic to Carboniferous accretionary orogen on the Northwest margin of Gondwana: The Journal of Geology, v. 117, p. 285–305, doi:10.1086/597472.

Cawood, P.A., 2005, The Terra Australis orogen: Rodinia break-up and development of the Pacific and Iapetus margins of Gondwana during the Neoproterozoic and Paleozoic: Earth-Science Reviews, v. 69, p. 249–279, doi:10.1016/j.earscirev.2004.09.001.

Cawood, P.A., and Buchan, C., 2007, Linking accretionary orogenesis with supercontinent assembly: Earth-Science Reviews, v. 82, p. 217–256, doi:10.1016/j.earscirev.2007.03.003.

Cawood, P.A., Kroner, A., Collins, W.J., Kusky, T.M., Mooney, W.D., and Windley, B.F., 2009, Accretionary orogens through Earth history, *in* Cawood, P.A., and Kroner, A., eds., Earth Accretionary Systems in Space and Time: Geological Society of London Special Publication 318, 36 p.

Cawood, P.A., Hawkesworth, C.J., and Dhuime, B., 2012, The continental record and the generation of continental crust: Geological Society of America Bulletin, v. 125, p. 14–32, doi:10.1130/B30722.1.

Cecil, R., Gehrels, G., Patchett, J., and Ducea, M., 2011, U-Pb-Hf characterization of the central Coast Mountains batholith: Implications for petrogenesis and crustal architecture: Lithosphere, v. 3, no. 4, p. 247–260, doi:10.1130/L134.1.

Cediel, F., Shaw, R., and Cáceres, C., 2003, Tectonic assembly of the northern Andean block, *in* Bartolini, C., Buffler, R.T., and Blickwede, J., eds., The Circum-Gulf of Mexico and the Caribbean: Hydrocarbon Habitats, Basin Formation and Plate Tectonics: American Association of Petroleum Geologists Memoir, v. 79, p. 815–848.

Chew, D.M., Schaltegger, U., Kosler, J., Whitehouse, M.J., Gutjahr, M., Spikings, R.A., and Miskovic, A., 2007a, U-Pb geochronologic evidence for the evolution of the Gondwanan margin of the north-central Andes: Geological Society of America Bulletin, v. 119, p. 697–711, doi:10.1130/B26080.1.

Chew, D.M., Kirkland, C.L., Schaltegger, U., and Goodhue, R., 2007b, Neoproterozoic glaciation in the Proto-Andes: Tectonic implications and global correlation: Geology, v. 35, p. 1095–1099, doi:10.1130/G23768A.1.

Chew, D.M., Magna, T., Kirkland, C.L., Miskovic, A., Cardona, A., Spikings, R., and Schaltegger, U., 2008, Detrital zircon fingerprint of the Proto-Andes: Evidence for a Neoproterozoic active margin?: Precambrian Research, v. 167, p. 186–200, doi:10.1016/j.precamres.2008.08.002.

Coira, B., Kay, S.M., Pérez, B., Woll, B., Hanning, M., and Flores, P., 1999, Magmatic sources and tectonic setting of Gondwana margin Ordovician magmas, northern Puna of Argentina and Chile, *in* Ramos, V., and Keppie, J., eds., Laurentia-Gondwana Connections before Pangea: Geological Society of America Special Paper 336, p. 145–170, doi:10.1130/0-8137-2336-1.145.

Collins, W.J., Belousova, E.A., Kempo, A.I.S., and Murphy, J.B., 2011, Two contrasting Phaneozoic orogenic systems revealed by hafnium isotope data: Nature Geoscience, v. 4, p. 333–337, doi:10.1038/ngeo1127.

Condie, K.C., 2014, Growth of continental crust: A balance between preservation and recycling: Mineralogical Magazine, v. 78, p. 623–637, doi:10.1180/minmag.2014.078.3.11.

Condie, K.C., Beyer, E., Belousova, E., Griffin, W.L., and O'Reilly, S.Y., 2005, U/Pb isotopic ages and Hf isotopic composition of single zircons: The search for juvenile Precambrian continental crust: Precambrian Research, v. 139, p. 42–100, doi:10.1016/j.precamres.2005.04.006.

Condie, K.C., Belousova, E., Griffin, W.L., and Sircombe, K.N., 2009, Granitoid events in space and time: Constraints from igneous and detrital zircon age spectra: Gondwana Research, v. 15, p. 228–242, doi:10.1016/j.gr.2008.06.001.

Condie, K.C., Bickford, M.E., Aster, R.C., Belousova, E., and Scholl, D.W., 2011, Episodic zircon ages, Hf isotopic composition and the preservation rate of continental crust: Geological Society of America Bulletin, v. 123, p. 951–957, doi:10.1130/B30344.1.

Coney, P.J., 1992, The Lachlan belt of eastern Australia and Circum-Pacific tectonic evolution: Tectonophysics, v. 214, p. 1–25, doi:10.1016/0040-1951(92)90187-B.

Cordani, U.G., 2009, From Rodinia to Gondwana: Tectonic significance of the Transbrasiliano Lineament: São Paulo, Simpósio 45 anos de geocronologia no Brasil, Boletim de Resumos Expandidos, p. 32–40.

Cordani, U.G., and Teixeira, W., 2007, Proterozoic accretionary belts in the Amazonian Craton, *in* Hatcher, R.D., Jr., Carlson, M.P., McBride, J.H., and Martínez Catalán, J.R., eds., Framework of Continental Crust: Geological Society of America Memoir 200, p. 297–320, doi:10.1130/2007.1200(14).

Cordani, U.G., Sato, K., Teixeira, W., Tassinari, C.C.G., and Basei, M.A.S., 2000, Crustal evolution of the South American Platform, *in* Cordani, U.G., Milani, E.J.,Thomaz-Filho, A., and Campos, D.A., eds., Tectonic Evolution of South America: Rio de Janeiro, 31st International Geological Congress, p. 19–40.

Cordani, U.G., Cardona, A., Jimenez, D., Liu, D., and Nutman, A.P., 2005, Geochronology of Proterozoic basement inliers from the Colombian Andes: Tectonic history of remnants from a fragmented Grenville belt, *in* Vaughan, A.P.M., Leat, P.T., and Pankhurst, R.J., eds., Terrane Processes at the Margins of Gondwana: Geological Society of London Special Publication 246, p. 329–346.

Cordani, U.G., Teixeira, W., D'Agrella-Filho, M.S., and Trindade, R.I., 2009, The position of the Amazonian Craton in supercontinents: Gondwana Research, v. 15, p. 396–407, doi:10.1016/j.gr.2008.12.005.

Cortés, M., Angelier, J., and Colletta, B., 2005, Paleostress evolution of the northern Andes (Eastern Cordillera of Colombia): Implications on plate kinematics of the South Caribbean region: Tectonics, v. 24, TC1008, doi:10.1029/2003TC001551.

Dalziel, I.W., de Wit, M.J., and Palmer, K.F., 1974, Fossil marginal basin in the southern Andes: Nature, v. 250, p. 291–294, doi:10.1038/250291a0.

Davies, J.H., and Stevenson, D.J., 1992, Physical model of source region of subduction zone volcanics: Journal of Geophysical Research. Solid Earth, v. 97, p. 2037–2070, doi:10.1029/91JB02571.

DeCelles, P.G., Ducea, M.N., Kapp, P., and Zandt, G., 2009, Cyclicity in Cordilleran orogenic systems: Nature Geoscience, v. 2, p. 251–257, doi:10.1038/ngeo469.

DeCelles, P.G., Zandt, G., Beck, S.L., Currie, C.A., Ducea, M.N., Kapp, P., Gehrels, G.E., Carrapa, B., Quade, J., and Schoenbohm, L.M., 2015, Cyclical orogenic processes in the central Cenozoic Andes, *in* DeCelles, P.G., Ducea, M.N., Carrapa, B., and Kapp, P.A. eds., Geodynamics of a Cordilleran Orogenic System: The Central Andes of Argentina and Northern Chile: Geological Society of America Memoir 212, p. 459–490, doi:10.1130/2015.1212(22).

Dhuime, B., Hawkesworth, C., and Cawood, P., 2011, When continents formed: Science, v. 331, p. 154–155, doi:10.1126/science.1201245.

Dickinson, W.R., 2008, Impact of differential zircon fertility of granitoid basement rocks in North America on age populations of detrital zircons and implications for granite petrogenesis: Earth and Planetary Science Letters, v. 275, p. 80–92, doi:10.1016/j.epsl.2008.08.003.

Ducea, M.N., Otamendi, J.E., Bergantz, G., Stair, K., Valencia, V., and Gehrels, G., 2010, Timing constraints on building an intermediate plutonic arc crustal section: U-Pb zircon geochronology of the Sierra Valle Fértil, Famatinian arc, Argentina: Tectonics, v. 29, TC4002, doi:10.1029/2009TC002615.

Ducea, M.N., Otamendi, J.E., Bergantz, G.W., Jianu, D., and Petrescu, L., 2015, The origin and petrologic evolution of the Ordovician Famatinian-Puna arc, *in* DeCelles, P.G., Ducea, M.N., Carrapa, B., and Kapp, P.A. eds., Geodynamics of a Cordilleran Orogenic System: The Central Andes of Argentina and Northern Chile: Geological Society of America Memoir 212, p. 125–138, doi:10.1130/2015.1212(07).

Einhorn, J.C., Gehrels, G.E., Vernon, A., and DeCelles, P.G., 2015, U-Pb zircon geochronology of Neoproterozoic–Paleozoic sandstones and Paleozoic plutonic rocks in the Central Andes (21°S–26°S), *in* DeCelles, P.G., Ducea, M.N., Carrapa, B., and Kapp, P.A., eds., Geodynamics of a Cordilleran Orogenic System: The Central Andes of Argentina and Northern Chile: Geological Society of America Memoir 212, p. 115–124, doi:10.1130/2015.1212(06).

Elliott, T., Plank, T., Zindler, A., White, W., and Bourdon, B., 1997, Element transport from slab to volcanic front at the Mariana arc: Journal of Geophysical Research. Solid Earth, v. 102, p. 14,991–15,019, doi:10.1029/97JB00788.

Escayola, M.P., Pimentel, M.M., and Armstrong, R., 2007, Neoproterozoic backarc basin: Sensitive high-resolution ion microprobe U-Pb and Sm-Nd isotopic evidence from the Eastern Pampean Ranges, Argentina: Geology, v. 35, p. 495–498, doi:10.1130/G23549A.1.

Finney, S., 2007, The parautochthonous Gondwanan origin of the Cuyania (greater Precordillera) terrane of Argentina: A re-evaluation of evidence used to support an allochthonous Laurentian origin: Geologica Acta, v. 5, p. 127–158.

Fisher, C.M., Vervoort, J.D., and DuFrane, S.A., 2014, Accurate Hf isotope determinations of complex zircons using the "laser ablation split stream" method: Geochemistry Geophysics Geosystems, v. 15, p. 121–139, doi:10.1002/2013GC004962.

Franz, G., Lucassen, F., Kramer, W., Trumbull, R., Romer, R., Wilke, H., Viramonte, J.G., Becchio, R., and Siebel, W., 2006, Crustal evolution at the Central Andean continental margin: A geochemical record of crustal growth, recycling and destruction, *in* Oncken, O., Chong, G., Franz, G., Giese, P., Götze, H.J., Ramos, V.A., Strecker, M.R., and Wigger, P., eds., The Andes: Active Subduction Orogeny (Frontiers in Earth Sciences): Berlin-Heidelberg, Springer, p. 45–64, doi:10.1007/978-3-540-48684-8_3.

Garzanti, E., Andò, S., and Vezzoli, G., 2009, Grain-size dependence of sediment composition and environmental bias in provenance studies: Earth and Planetary Science Letters, v. 277, p. 422–432, doi:10.1016/j.epsl.2008.11.007.

Gehrels, G., 2012, Detrital zircon U-Pb geochronology: Current methods and new opportunities, *in* Busby, C., and Azor, A., eds., Tectonics of Sedimentary Basins: Recent Advances: Wiley-Blackwell Publishing, p. 45–62, doi:10.1002/9781444347166.ch2.

Gehrels, G., and Pecha, M., 2014, Detrital zircon U-Pb geochronology and Hf isotope geochemistry of Paleozoic and Triassic passive margin strata of western North America: Geosphere, v. 10, p. 49–65, doi:10.1130/GES00889.1.

Gehrels, G., Rusmore, M., Woodsworth, G., Crawford, M., Andronicos, C., Hollister, L., Patchett, J., Ducea, M., Butler, R., Klepeis, K., Davidson, C., Mahoney, B., Friedman, R., Haggart, J., Crawford, W., Pearson, D., and Girardi, J., 2009, U-Th-Pb geochronology of the Coast Mountains Batholith in north-coastal British Columbia: Constraints on age, petrogenesis, and tectonic evolution: Geological Society of America Bulletin, v. 121, p. 1341–1361, doi:10.1130/B26404.1.

Gehrels, G.E., 2000, Introduction to detrital zircon studies of Paleozoic and Triassic strata in western Nevada and northern California, *in* Soreghan, M.J. and Gehrels, G.E., eds., Paleozoic and Triassic Paleogeography and Tectonics of Western Nevada and Northern California: Geological Society of America Special Paper 347, p. 1–17, doi:10.1130/0-8137-2347-7.1.

Gehrels, G.E., 2014, Detrital zircon U-Pb geochronology applied to tectonics: Annual Review of Earth and Planetary Sciences, v. 42, p. 127–149, doi:10.1146/annurev-earth-050212-124012.

Gehrels, G.E., Valencia, V., and Pullen, A., 2006, Detrital zircon geochronology by Laser-Ablation Multicollector ICPMS at the Arizona LaserChron Center, *in* Loszewski, T., and Huff, W., eds.,

Geochronology: Emerging Opportunities, Paleontology Society Short Course: Paleontology Society Papers, v. 11, p. 1–10.
Gehrels, G.E., Valencia, V., and Ruiz, J., 2008, Enhanced precision, accuracy, efficiency, and spatial resolution of U-Pb ages by laser ablation–multicollector–inductively coupled plasma–mass spectrometry: Geochemistry Geophysics Geosystems, v. 9, Q03017, doi:10.1029/2007GC001805.
Gibert, G., Gerbault, M., Hassani, R., and Tric, E., 2012, Dependency of slab geometry on absolute velocities and conditions for cyclicity: Insights from numerical modeling: Geophysical Journal International, v. 189, p. 747–760, doi:10.1111/j.1365-246X.2012.05426.x.
Goodwin, A.M., 1996, Principles of Precambrian geology: New York, Academic Press, 327 p.
Grinsted, A., Moore, J.C., and Jevrejeva, S., 2004, Application of the cross wavelet transform and wavelet coherence to geophysical time series: Nonlinear Processes in Geophysics, v. 11, p. 561–566, doi:10.5194/npg-11-561-2004.
Haschke, M., Gunther, A., Melnick, D., Echtler, H., Reutter, K.J., Scheuber, E., and Oncken, O., 2006, Central and southern Andean tectonic evolution inferred from arc magmatism, *in* Oncken, O., Chong, G., Franz, G., Giese, P., Götze, H.-J., Ramos, H.-J., Strecker, M.R., and Wigger, P., eds., The Andes—Active Subduction Orogeny: Frontiers in Earth Sciences: Berlin, Springer-Verlag, v. 1, p. 337–353.
Haschke, M.R., Scheuber, E., Günther, A., and Reutter, K.J., 2002, Evolutionary cycles during the Andean orogeny: Repeated slab breakoff and flat subduction?: Terra Nova, v. 14, p. 49–55, doi:10.1046/j.1365-3121.2002.00387.x.
Hawkesworth, C., Cawood, P., Kemp, T., Storey, C., and Dhuime, B., 2009, A matter of preservation: Science, v. 323, p. 49–50, doi:10.1126/science.1168549.
Hawkesworth, C., Dhuime, B., Pietranik, A., Cawood, P., Kemp, T., and Storey, C., 2010, The generation and evolution of the continental crust: Journal of the Geological Society of London, v. 167, p. 229–248, doi:10.1144/0016-76492009-072.
Hervé, F., Pankhurst, R.J., Fanning, C.M., Calderón, M., and Yaxley, G.M., 2007, The South Patagonian batholith: 150 my of granite magmatism on a plate margin: Lithos, v. 97, p. 373–394, doi:10.1016/j.lithos.2007.01.007.
Ibanez-Mejia, M., Ruiz, J., Valencia, V.A., Cardona, A., Gehrels, G.E., and Mora, A.R., 2011, The Putumayo orogen of Amazonia and its implications for Rodinia reconstructions: New U-Pb geochronological insights into the Proterozoic tectonic evolution of northwestern South America: Precambrian Research, v. 191, p. 58–77, doi:10.1016/j.precamres.2011.09.005.
Iizuka, T., Komiya, T., Rino, S., Maruyama, S., and Hirata, T., 2010, Detrital zircon evidence for Hf isotopic evolution of granitic crust and continental growth: Geochimica et Cosmochimica Acta, v. 74, p. 2450–2472, doi:10.1016/j.gca.2010.01.023.
Jiménez-Mejía, D.M., Juliani, C., and Cordani, U.G., 2006, P-T-t conditions of high-grade metamorphic rocks of the Garzon Massif, Andean basement, SE Colómbia: Journal of South American Earth Sciences, v. 21, p. 322–336, doi:10.1016/j.jsames.2006.07.001.
Jordan, T.E., and Allmendinger, R.W., 1986, The Sierras Pampeanas of Argentina: A modern analogue of Rocky Mountain foreland deformation: American Journal of Science, v. 286, p. 737–764, doi:10.2475/ajs.286.10.737.
Kay, S.M., Godoy, E., and Kurtz, A., 2005, Episodic arc migration, crustal thickening, subduction erosion, and magmatism in the south-central Andes: Geological Society of America Bulletin, v. 117, p. 67–88, doi:10.1130/B25431.1.
Kemp, A.I.S., Hawkesworth, C.J., Collins, W.J., Cray, C.M., and Blevin, P.L., 2009, Isotopic evidence for rapid continental growth in an extensional accretionary orogen: The Tasmanides, eastern Australia: Earth and Planetary Science Letters, v. 284, p. 455–466, doi:10.1016/j.epsl.2009.05.011.
Kennan, L., and Pindell, J.L., 2009, Dextral shear, terrane accretion and basin formation in the Northern Andes: Best explained by interaction with a Pacific-derived Caribbean plate?: Geological Society of London Special Publication 328, p. 487–531, doi:10.1144/SP328.20.
Kröner, A., and Cordani, U., 2003, African, southern Indian and South American cratons were not part of the Rodinia supercontinent: Evidence from field relationships and geochronology: Tectonophysics, v. 375, p. 325–352, doi:10.1016/S0040-1951(03)00344-5.
Lawrence, R.L., Cox, R., Mapes, R.W., and Coleman, D.S., 2011, Hydrodynamic fractionation of zircon age populations: Geological Society of America Bulletin, v. 123, p. 295–305, doi:10.1130/B30151.1.
Lee, C., and King, S.D., 2011, Dynamic buckling of subducting slabs reconciles geological and geophysical observations: Earth and Planetary Science Letters, v. 312, p. 360–370, doi:10.1016/j.epsl.2011.10.033.
Link, P.K., Fanning, M.C., and Beranek, L.P., 2005, Reliability and longitudinal change of detrital-zircon age spectra in the Snake River system, Idaho and Wyoming: An example of reproducing the bumpy barcode: Sedimentary Geology, v. 182, p. 101–142, doi:10.1016/j.sedgeo.2005.07.012.
Litherland, M., and Power, G., 1989, The geologic and geomorphologic evolution of Serrania Huanchaca, eastern Bolivia: The legendary "Lost World": Journal of South American Earth Sciences, v. 2, p. 1–17, doi:10.1016/0895-9811(89)90023-0.
Loewy, S.L., Connelly, J.N., and Dalziel, I.W.D., 2004, An orphaned basement block: The Arequipa-Antofalla basement of the central Andean margin of South America: Geological Society of America Bulletin, v. 116, p. 171–187, doi:10.1130/B25226.1.
Lomb, N.R., 1976, Least-squares frequency analysis of unequally spaced data: Astrophysics and Space Science, v. 39, p. 447–462, doi:10.1007/BF00648343.
Ludwig, K.R., 2008, Isoplot 3.60: Berkeley Geochronology Center, Special Publication, no. 4, 77 p.
Maloney, K.T., Clarke, G.L., Klepeis, K.A., and Quevedo, L., 2013, The Late Jurassic to present evolution of the Andean margin: Drivers and the geological record: Tectonics, v. 32, p. 1049–1065, doi:10.1002/tect.20067.
Mapes, R.W., Coleman, D.S., and Nogueira, A.C.R., 2005, Understanding zircon transport in the modern Amazon River: Geological Society of America Abstracts with Programs, v. 37, no. 4, p. 86.
McCourt, W.J., Aspden, J.A., and Brook, M., 1984, New geological and geochronological data from the Colombian Andes: Continental growth by multiple accretion: Journal of the Geological Society of London, v. 141, p. 831–845, doi:10.1144/gsjgs.141.5.0831.
Milliman, J.D., and Syvitski, J.P., 1992, Geomorphic/tectonic control of sediment discharge to the ocean: The importance of small mountainous rivers: The Journal of Geology, v. 100, p. 525–544, doi:10.1086/629606.
Miskovic, A., Spikings, R.A., Chew, D.M., Koaler, J., Ulianov, A., and Schaltegger, U., 2009, Tectonomagmatic evolution of Western Amazonia: Geochemical characterization and zircon U-Pb geochronologic constraints from the Peruvian Eastern Cordilleran granitoids: Geological Society of America Bulletin, v. 121, p. 1298–1324, doi:10.1130/B26488.1.
Moecher, D.P., and Samson, S.D., 2006, Differential zircon fertility of source terranes and natural bias in the detrital zircon record: Implications for sedimentary provenance analysis: Earth and Planetary Science Letters, v. 247, p. 252–266, doi:10.1016/j.epsl.2006.04.035.
Ordóñez-Carmona, O., Restrepo Álvarez, J.J., and Pimentel, M.M., 2006, Geochronological and isotopical review of pre-Devonian crustal basement of the Colombian Andes: Journal of South American Earth Sciences, v. 21, p. 372–382, doi:10.1016/j.jsames.2006.07.005.
Pankhurst, R.J., Rapela, C.W., Saavedra, J., Baldo, E., Dahlquist, J., Pascua, I., and Fanning, C.M., 1998, The Famatinian magmatic arc in the central Sierras Pampeanas: An Early to Mid-Ordovician continental arc on the Gondwana margin, *in* Pankhurst, R.J., and Rapela, C.W., eds., The Proto-Andean Margin of Gondwana: Geological Society of London Special Publication 142, p. 343–368.
Pankhurst, R.J., Weaver, S.D., Hervé, F., and Larrondo, P., 1999, Mesozoic–Cenozoic evolution of the North Patagonian batholith in Aysen, southern Chile: Journal of the Geological Society of London, v. 156, p. 673–694, doi:10.1144/gsjgs.156.4.0673.
Pankhurst, R.J., Riley, T.R., Fanning, C.M., and Kelley, S.P., 2000, Episodic silicic volcanism in Patagonia and the Antarctic Peninsula: Chronology of magmatism associated with the break-up of Gondwana: Journal of Petrology, v. 41, p. 605–625, doi:10.1093/petrology/41.5.605.
Pankhurst, R.J., Rapela, C.W., Fanning, C.M., and Márquez, M., 2006, Gondwanide continental collision and the origin of Patagonia: Earth-Science Reviews, v. 76, p. 235–257, doi:10.1016/j.earscirev.2006.02.001.
Patchett, P.J., 1983, Importance of the Lu-Hf isotopic system in studies of planetary chronology and chemical evolution: Geochimica et Cosmochimica Acta, v. 47, p. 81–91, doi:10.1016/0016-7037(83)90092-3.
Patchett, P.J., and Tatsumoto, M., 1980, Hafnium isotope variations in oceanic basalts: Geophysical Research Letters, v. 7, p. 1077–1080, doi:10.1029/GL007i012p01077.
Paterson, S.R., and Ducea, M.N., 2015, Arc magmatic tempos: Gathering the evidence: Elements v. 11, no. 2, p. 91–98, doi:10.2113/gselements.11.2.91.
Rainbird, R., Cawood, P., and Gehrels, G., 2012, The Great Grenvillian Sedimentation Episode: Record of Supercontinent Rodinia's assembly, *in* Busby, C., and Azor, A., eds., Tectonics of Sedimentary Basins: Recent Advances: Wiley-Blackwell Publishing, p. 583–601, doi:10.1002/9781444347166.ch29.

Ramos, V.A., 2004, Cuyania, an exotic block to Gondwana: Review of a historical success and the present problems: Gondwana Research, v. 7, p. 1009–1026, doi:10.1016/S1342-937X(05)71081-9.

Ramos, V.A., 2008, The basement of the Central Andes: The Arequipa and related terranes: Annual Review of Earth and Planetary Sciences, v. 36, p. 289–324, doi:10.1146/annurev.earth.36.031207.124304.

Ramos, V.A., 2009, Anatomy and global context of the Andes: Main geologic features and the Andean orogenic cycle, *in* Kay, S.M., Ramos, V.A., and Dickinson, W.R., eds., Backbone of the Americas: Shallow Subduction, Plateau Uplift, and Ridge and Terrane Collision: Geological Society of America Memoir 204, p. 31–65, doi:10.1130/2009.1204(02).

Ramos, V.A., 2010, The tectonic regime along the Andes: Present settings as a key for the Mesozoic regimes: Geological Journal, v. 45, p. 2–25.

Ramos, V.A., Litvak, V.D., Folguera, A., and Spagnuolo, M., 2014, An Andean tectonic cycle: From crustal thickening to extension in a thin crust (34°–37°SL): Geoscience Frontiers, v. 5, no. 3, p. 351–367, doi:10.1016/j.gsf.2013.12.009.

Rapela, C.W., Coira, B., Toselli, A., and Saavedra, J., 1992, The Lower paleozoic magmatism of south-western Gondwana and the evolution of the Famatinian Orogen: International Geology Review, v. 34, p. 1081–1142, doi:10.1080/00206819209465657.

Rapela, C.W., Pankhurst, R.J., Casquet, C., Baldo, E., Saavedra, J., Galindo, C., and Fanning, C.M., 1998, The Pampean orogeny of the southern proto-Andes: Evidence for Cambrian continental collision in the Sierras de Córdoba, *in* Pankhurst, R.J., and Rapela, C.W., eds., The Proto-Andean Margin of Gondwana: Geological Society of London Special Publication 142, p. 181–217.

Rapela, C.W., Pankhurst, R.J., Casquet, C., Fanning, C.M., Baldo, E.G., González-Casado, J.M., Galindo, C., and Dahlquist, J., 2007, The Río de la Plata craton and the assembly of SW Gondwana: Earth-Science Reviews, v. 83, p. 49–82, doi:10.1016/j.earscirev.2007.03.004.

Restrepo-Pace, P.A., Ruiz, J., Gehrels, G., and Cosca, M., 1997, Geochronology and Nd isotopic data of Grenville-age rocks in the Colombian Andes: New constraints for Late Proterozoic–Early Paleozoic paleocontinental reconstructions of the Americas: Earth and Planetary Science Letters, v. 150, p. 427–441, doi:10.1016/S0012-821X(97)00091-5.

Rino, S., Komiya, T., Windley, B.F., Katayama, I., Motoki, A., and Hirata, T., 2004, Major episodic increase of continental crustal growth determined from zircon ages of river sands; implications for mantle overturns in the Early Precambrian: Physics of the Earth and Planetary Interiors, v. 146, p. 369–394, doi:10.1016/j.pepi.2003.09.024.

Rino, S., Kon, Y., Sato, W., Maruyama, S., Santosh, M., and Zhao, D., 2008, The Grenvillian and Pan-African orogens: World's largest orogenies through geologic time, and their implications on the origin of superplumes: Gondwana Research, v. 14, p. 51–72, doi:10.1016/j.gr.2008.01.001.

Rossel, P., Oliveros, V., Ducea, M.N., Charrier, R., Scaillet, S., Retamal, L., and Figueroa, O., 2013, The Early Andean subduction system as an analog to island arcs: Evidence from across-arc geochemical variations in northern Chile: Lithos, v. 179, p. 211–230, doi:10.1016/j.lithos.2013.08.014.

Rubatto, D., 2002, Zircon trace element geochemistry: partitioning with garnet and the link between U-Pb ages and metamorphism: Chemical Geology, v. 184, p. 123–138, doi:10.1016/S0009-2541(01)00355-2.

Ruiz, J., Tosdal, R.M., Restrepo, P.A., and Murillo-Muñeton, G., 1999, Pb Isotope evidence for Colombian-southern Mexico connections in the Proterozoic, *in* Ramos, V.A., and Keppie, J.D., eds., Laurentia and Gondwana Connections before Pangea: Geological Society of America Special Paper 336, p. 183–197, doi:10.1130/0-8137-2336-1.183.

Salfity, J.A., and Marquillas, R.A., 1994, Tectonic and sedimentary evolution of the Cretaceous–Eocene Salta Group basin, Argentina, *in* Salfity, J.A., ed., Cretaceous Tectonics of the Andes: Braunschweig, Vieweg, p. 266–315, doi:10.1007/978-3-322-85472-8_6.

Santos, J.O.S., Hartmann, L.A., Gaudette, H.E., Groves, D.I., Mcnaughton, N.J., and Fletcher, I.R., 2000, A new understanding of the provinces of the Amazon Craton based on integration of field mapping and U-Pb and Sm-Nd geochronology: Gondwana Research, v. 3, p. 453–488, doi:10.1016/S1342-937X(05)70755-3.

Santos, J.O.S., Rizzotto, G.J., Potter, P.E., McNaughton, N.J., Matos, R.S., Hartmann, L.A., Chemale, F., and Quadros, M.E.S., 2008, Age and autochthonous evolution of the Sunsás orogen in West Amazon Craton based on mapping and U-Pb geochronology: Precambrian Research, v. 165, p. 120–152, doi:10.1016/j.precamres.2008.06.009.

Scargle, J.D., 1982, Studies in astronomical time series analysis. II. Statistical aspects of spectral analysis of unevenly spaced data: The Astrophysical Journal, v. 263, p. 835–853, doi:10.1086/160554.

Scherer, E., Münker, C., and Mezger, K., 2001, Calibration of the lutetium-hafnium clock: Science, v. 293, p. 683–687, doi:10.1126/science.1061372.

Shackleton, R.M., Ries, A.C., Coward, M.P., and Cobbold, P.R., 1979, Structure, metamorphism and geochronology of the Arequipa Massif of coastal Peru: Journal of the Geological Society of London, v. 136, p. 195–214, doi:10.1144/gsjgs.136.2.0195.

Slama, J., Koaler, J., Condon, D.J., Crowley, J.L., Gerdes, A., Hanchar, J.M., Horstwood, M.S.A., Morris, G.A., Nasdala, L., Norberg, N., Schaltegger, U., Schoene, B., Tubrett, M.N., and Whitehouse, M.J., 2008, Plesovice zircon—A new natural reference material for U-Pb and Hf isotopic microanalysis: Chemical Geology, v. 249, p. 1–35, doi:10.1016/j.chemgeo.2007.11.005.

Söderlund, U., Patchett, P.J., Vervoort, J.D., and Isachsen, C.E., 2004, The ^{176}Lu decay constant determined by Lu-Hf and U-Pb isotope systematics of Precambrian mafic intrusions: Earth and Planetary Science Letters, v. 219, p. 311–324, doi:10.1016/S0012-821X(04)00012-3.

Speer, J.A., 1982, Zircon: Mineralogical Society of America Reviews in Mineralogy, v. 5, p. 67–112.

Stern, C.R., and De Wit, M.J., 2003, Rocas Verdes ophiolites, southernmost South America: Remnants of progressive stages of development of oceanic-type crust in a continental margin back-arc basin: Geological Society of London Special Publication 218, p. 665–683, doi:10.1144/GSL.SP.2003.218.01.32.

Strecker, M.R., Cerveny, P., Bloom, A.L., and Malizia, D., 1989, Late Cenozoic tectonism and landscape development in the foreland of the Andes: Northern Sierras Pampeanas (26°–28° S), Argentina: Tectonics, v. 8, p. 517–534, doi:10.1029/TC008i003p00517.

Tassinari, C.C., and Macambira, M.J., 1999, Geochronological provinces of the Amazonian Craton: Episodes, v. 22, p. 174–182.

Teixeira, W., Tassinari, C.G., Cordani, U.G., and Kawashita, K., 1989, A review of the geochronology of the Amazonian Craton: Tectonic implications: Precambrian Research, v. 42, p. 213–227, doi:10.1016/0301-9268(89)90012-0.

Teixeira, W., Geraldes, M.C., Matos, R., Ruiz, A.S., Saes, G., and Vargas-Mattos, G., 2010, A review of the tectonic evolution of the Sunsás belt, SW Amazonian Craton: Journal of South American Earth Sciences, v. 29, p. 47–60, doi:10.1016/j.jsames.2009.09.007.

Thomas, W.A., Astini, R.A., Mueller, P.A., Wooden, J.L., and Gehrels, G., 2004, Transfer of the Argentine Precordillera terrane from Laurentia: Constraints from detrital-zircon geochronology: Geology, v. 32, p. 965–968, doi:10.1130/G20727.1.

Torrence, C., and Compo, G.P., 1998, A practical guide to wavelet analysis: Bulletin of the American Meteorological Society, v. 79, p. 61–78, doi:10.1175/1520-0477(1998)079<0061:APGTWA>2.0.CO;2.

Valeriano, C.M., Pimentel, M.M., Heilbron, M., Almeida, J.C.H., and Trouw, R.A.J., 2008, Tectonic evolution of the Brasília Belt, Central Brazil, and early assembly of Gondwana: Geological Society of London Special Publication 294, p. 197–210, doi:10.1144/SP294.11.

Vervoort, J.D., and Blichert-Toft, J., 1999, Evolution of the depleted mantle: Hf isotope evidence from juvenile rocks through time: Geochimica et Cosmochimica Acta, v. 63, p. 533–556, doi:10.1016/S0016-7037(98)00274-9.

Vervoort, J.D., and Patchett, P.J., 1996, Behavior of hafnium and neodymium isotopes in the crust: Constraints from crustally derived granites: Geochimica et Cosmochimica Acta, v. 60, no. 19, p. 3717–3733, doi:10.1016/0016-7037(96)00201-3.

Vervoort, J.D., Patchett, P.J., Blichert-Toft, J., and Albarède, F., 1999, Relationships between Lu-Hf and Sm-Nd isotopic systems in the global sedimentary system: Earth and Planetary Science Letters, v. 168, p. 79–99, doi:10.1016/S0012-821X(99)00047-3.

Vervoort, J.D., Patchett, P.J., Soderlund, U., and Baker, M., 2004, Isotopic composition of Yb and the determination of Lu concentrations and Lu/Hf ratios by isotope dilution using MC-ICPMS: Geochemistry Geophysics Geosystems, v. 5, no. 11, doi:10.1029/2004GC000721.

Voice, P.J., Kowalewski, M., and Eriksson, K.A., 2011, Quantifying the timing and rate of crustal evolution: Global compilation of radiometrically dated detrital zircon grains: The Journal of Geology, v. 119, p. 109–126, doi:10.1086/658295.

Wessel, P., Smith, W.H.F., Scharroo, R., Luis, J., and Wobbe, F., 2013, Generic Mapping Tools: Improved Version Released: Eos (Transactions, American Geophysical Union), v. 94, no. 45, p. 409, doi:10.1002/2013EO450001.

Willner, A.P., Gerdes, A., and Massonne, H.J., 2008, History of crustal growth and recycling at the Pacific convergent margin of South America at latitudes 29°–36°S revealed by a U-Pb and Lu-Hf isotope study of detrital zircon from late Paleozoic accretionary systems: Chemical Geology, v. 253, p. 114–129, doi:10.1016/j.chemgeo.2008.04.016.

Windley, B.F., 1995, The Evolving Continents: New York, John Wiley and Sons, 526 p.

Woodhead, J.D., and Hergt, J.M., 2005, A preliminary appraisal of seven natural zircon reference materials for in situ Hf isotope determination: Geostandards and Geoanalytical Research, v. 29, p. 183–195, doi:10.1111/j.1751-908X.2005.tb00891.x.